Understanding Robust Learning through the Lens of Representation Similarities

Christian Cianfarani*
Department of Computer Science
University of Chicago

Arjun Nitin Bhagoji*
Department of Computer Science
University of Chicago

Vikash Sehwag*
Department of ECE
Princeton University

Ben Zhao
Department of Computer Science
University of Chicago

Haitao Zheng
Department of Computer Science
University of Chicago

Prateek Mittal
Department of ECE
Princeton University

Abstract

Representation learning, *i.e.* the generation of representations useful for downstream applications, is a task of fundamental importance that underlies much of the success of deep neural networks (DNNs). Recently, *robustness to adversarial examples* has emerged as a desirable property for DNNs, spurring the development of robust training methods that account for adversarial examples. In this paper, we aim to understand how the properties of representations learned by robust training differ from those obtained from standard, non-robust training. This is critical to diagnosing numerous salient pitfalls in robust networks, such as, degradation of performance on benign inputs, poor generalization of robustness, and increase in over-fitting. We utilize a powerful set of tools known as representation similarity metrics, across three vision datasets, to obtain layer-wise comparisons between robust and non-robust DNNs with different training procedures, architectural parameters and adversarial constraints. Our experiments highlight hitherto unseen properties of robust representations that we posit underlie the behavioral differences of robust networks. We discover a lack of specialization in robust networks' representations along with a disappearance of 'block structure'. We also find overfitting during robust training largely impacts deeper layers. These, along with other findings, suggest ways forward for the design and training of better robust networks.

1 Introduction

Representation learning is fundamental to machine learning and a task on which deep neural networks perform remarkably well. Given complex high-dimensional input signals, such as images, speech, or text, deep neural networks (DNNs) can learn meaningful, lower-dimensional representations [33, 6, 57, 13, 24, 12, 66]. The downstream utility of these representations underlies DNNs' success on different tasks [5, 15, 51, 36, 3]. For standard image classification, neural networks learn well-separated representations of inputs from different classes to achieve high accuracy. The discovery of adversarial examples [4, 54], perturbed inputs that induce high error in model predictions (even for well-trained classifiers) has motivated the need for another desirable property: *adversarial robustness*. Robust training methods typically protect against adversarial examples during the training phase by converting the standard empirical risk minimization objective to a min-max one (Figure 1) [35, 46, 65]. However, they typically have far worse performance on benign inputs, converge

*Equal Contribution

36th Conference on Neural Information Processing Systems (NeurIPS 2022).

slower and appear to require larger architectures to be effective [17, 38, 56, 60]. Given the importance of representation learning for good downstream performance, we posit that an effective method to identify potential improvements for robust training is via developing a better understanding of robustly learned representations [2].

Our approach is to juxtapose representations of non-robust and robust networks and analyze them through a unified lens. Aggregate metrics like loss and accuracy do shed some light on the differences, but these are task-driven and do not admit a layer-wise comparison of representations [1, 20]. We need a comprehensive analysis of the impact of choice of architectural parameters like depth and width, nature of the threat model and corresponding attack strength, and the choice of dataset on robustly learned representations and their link to downstream performance.

To this end, we leverage recent work on representation similiarity (RS) that enables fine-grained comparisons of representations obtained across all layers in a deep neural network (DNN) [31, 44]. Our key findings, using both benign and adversarial inputs as probes over CIFAR-10 [32] and the Imagenette and Imagewoof [25] subsets of the Imagenet [10] dataset, are:

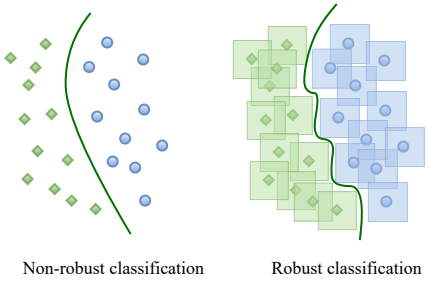

Figure 1: **Non-robust vs robust training.** Adversarially robust training aims to learn decision boundaries that are robust to adversarial perturbations (ℓ_∞ in this sketch), naturally learning more complex decision boundaries than non-robust training.

Robust representations are less specialized (§3): Robust networks exhibit much higher similarity across spatially distant layers compared to non-robust networks, which have far more localized similarity. The latter thus exhibit the expected specialization in layers, which is unexpectedly missing in the former. Further, we find reducing the width of the network has a similar effect to increasing the budget used in robust training, with both changes increasing long-range similarity among the learned representations. This indicates that the relative capacity of a network drops as the budget is increased.

Early layers are largely unaffected by adversarial examples (§4): The representations of perturbed inputs from non-robust and robust networks are, as expected, starkly different. On the other hand, the representations of benign and perturbed inputs from robust networks are indistinguishable from one another with regards to representation similarity metrics.

Deeper layers overfit (§5): For both non-robust and robust training, early layers in the network converge within the first few epochs, and exhibit very little variation in subsequent training. This indicates they perform similar roles in both benign and robust networks. Deeper layers converge slower while visiting drastically different representations over the course of training. These different representations usually occur when the loss indicates overfitting, leading us to conclude that *deeper layers overfit during robust training*.

Visually dissimilar adversarial constraints can lead to similar robust representations (§6): Regardless of the adversarial constraint, we find a high degree of similarity between the representations of perturbed and benign inputs for robust networks. Representations from networks robust to different, but allied (*e.g.* ℓ_p), threat models are similar across attack strength. We find surprising similarities between the representations of visually unrelated threat models at lower attack strengths.

What do our findings imply? The lack of specialization in robust networks even with heavily overparametrized architectures suggests a need for explicit tools to differentiate between layers during training. Further, the overfitting we find in deeper layers of neural networks is an indication that layer-wise specialized regularization methods need to be adopted for robust training. We hope the lessons from this paper and our accompanying website [3] with open-sourced code spur the development of robust learning-specific architectures and training methods.

Paper Layout. We provide an overview of RS tools and robust training methods in §2. We compare representations from non-robust and robust networks using benign inputs in §3. §4 repeats this

[2] We note that we use the word 'robust' as shorthand for 'adversarially robust' throughout the paper. When considering other types of robustness, such as to common corruptions, we explicitly mention it.

[3] `https://robustrs.github.io/`

Network	Benign accuracy			Robust accuracy		
	Train	Test	Δ	Train	Test	Δ
Non-robust	100.0%	94.9%	5.1%	0.0%	0.0%	0.0%
Robust	100.0%	87.6%	12.4%	98.2%	44.2%	54.0%

Table 1: Performance of non-robust and robust Wide Resnet 28-10 (WRN-28-10) on the CIFAR-10 dataset. Note, in particular, the high generalization gap in robust networks .

analysis with perturbed inputs. The evolution of robust representations over training is studied in §5 while the impact of different threat models is in §6. §7 discusses lessons and limitations.

2 Background and Setup

We provide a brief overview of the techniques we use to train robust networks and the tools we use to probe the intermediate representations of neural networks. Further background and related work is in Appendix A.

2.1 Adversarial Examples and Robust Learning

Adversarial examples are perturbed inputs to machine learning models that intentionally induce misclassification [4, 54]. For an input $\mathbf{x}$, an untargeted adversarial example with respect to a model f and loss function $\ell(\cdot)$ is generated by adding a perturbation $\boldsymbol{\delta}$ such that $\boldsymbol{\delta} = \arg\max_{\mathbf{x}+\boldsymbol{\delta}\in N(\mathbf{x})} \ell(f(\mathbf{x}+\boldsymbol{\delta}), y)$, where y is the label of the original class and $N(\cdot)$ represents the adversarial constraint or neighborhood. The most commonly used constraints are L_p-ball based, although we also experiment with other unrelated classes of attacks, such as JPEG, Gabor, or Snow based perturbations [28]. We characterize activations of internal layer in a network as: 1) *Benign representation:* if input is non-adversarial 2) *Adversarial representation:* if input is an adversarial example.

Adversarial training [35] has emerged as the most effective methods to train robust classifiers [7], where it accounts for adversarial examples during training. It modifies the empirical risk minimization procedure in non-robust training to a min-max optimization, where the inner maximization focuses on finding the strongest adversarial example for each input during training:

$$\min_{\theta} \mathbb{E}_{(\mathbf{x},y)\in\mathcal{D}} \left[\max_{\mathbf{x}+\boldsymbol{\delta}\in N(\mathbf{x})} \ell(f_\theta(\mathbf{x}+\boldsymbol{\delta}), y) \right], \tag{1}$$

where $\mathcal{D}$ is a data distribution and f_θ is a model with parameters θ. Newer methods, like TRADES [65], attempt to improve on adversarial training by better balancing the tradeoff between robustness and accuracy. We refer to models trained using methods that account for adversarial examples as *robust* models and those trained without these methods as *non-robust* models.

We refer to accuracy on non-perturbed input as *benign accuracy* and on adversarial examples as *robust accuracy*. Adversarial training is well known to trade-off benign accuracy to gain robustness and exhibits a high generalization gap in robust accuracy (as we show in Table 1 for the CIFAR-10 dataset).

2.2 Probing Neural Network Representations

Representation similarity (RS) metrics allow for the quantitative comparison of the activations of different sets of neurons on a given dataset. Comparing learned, internal representations within and between neural networks of different architectures is important for understanding the performance and behavior of these networks under changing conditions. Several metrics have been proposed for this purpose: Canonical Correlation Analysis (CCA) [22] and its extensions, Singular Vector CCA (SVCCA) [44] and Projection Weighted CCA (PWCCA) [37], Centered Kernel Alignment (CKA) [31], the Orthogonal Procrustes distance [14] and model stitching [2, 9]. These metrics can all handle different sized representations, but require that the number of datapoints be the same. Other work has used the fitting of sparse linear layers to understand the behavior of deeper layer representations [59, 47].

We choose CKA to measure representation similarity, due to its desirable properties such as orthogonal and isotropic invariance, and wide use in previous work [40, 42, 43, 58]. We also find CKA to be computationally more efficient ($10\times$ and $30\times$ faster than Procrustes and SVCCA respectively), while yielding similar high-level insights (see Appendix B.1). Ding et al. [14] have shown that CKA is insensitive to deletions of principal components of representations that strongly correlate with model accuracy. However, since we do not compare neural networks with representations of reduced dimensions, this does not affect our results.

Centred Kernel Alignment (CKA): Let $\boldsymbol{X} \in \mathbb{R}^{n \times p_1}$ with rows $\boldsymbol{x}_i$, and $\boldsymbol{Y} \in \mathbb{R}^{n \times p_2}$ with rows $\boldsymbol{y}_i$ be the activation matrices of layers with p_1 and p_2 neurons respectively, defined on the same set of n points. These activation matrices are then the representations induced by a particular layer. We also define a $n \times n$ centering matrix $\boldsymbol{H} = \boldsymbol{I}_n - \mathbf{1}\mathbf{1}^\top$. The CKA between these activation matrices is then

$$\text{CKA}(\boldsymbol{K}, \boldsymbol{L}) = \frac{\text{tr}(\boldsymbol{K}\boldsymbol{H}\boldsymbol{L}\boldsymbol{H})}{\sqrt{\text{tr}(\boldsymbol{K}\boldsymbol{H}\boldsymbol{K}\boldsymbol{H})\text{tr}(\boldsymbol{L}\boldsymbol{H}\boldsymbol{L}\boldsymbol{H})}}, \tag{2}$$

where $\boldsymbol{K}_{ij} = k(\boldsymbol{x}_i, \boldsymbol{x}_j)$, $\boldsymbol{L}_{ij} = l(\boldsymbol{y}_i, \boldsymbol{y}_j)$, with k and l being kernels. When the kernels are linear and the activation matrices are centered, we get the Linear CKA between activation matrices to be

$$\text{Linear CKA} = \frac{\|\boldsymbol{Y}^\top \boldsymbol{X}\|_F^2}{\|\boldsymbol{X}^\top \boldsymbol{X}\|_F \|\boldsymbol{Y}^\top \boldsymbol{Y}\|_F} = \frac{\langle \text{vec}(\boldsymbol{X}\boldsymbol{X}^\top), \text{vec}(\boldsymbol{Y}\boldsymbol{Y}^\top) \rangle}{\|\boldsymbol{X}^\top \boldsymbol{X}\|_F \|\boldsymbol{Y}^\top \boldsymbol{Y}\|_F}. \tag{3}$$

Since Kornblith et al. [31] find the use of a linear kernel to be as accurate as and much faster than the RBF kernel, we focus only on linear kernels. To reduce memory usage, we use online CKA which uses batching to get an unbiased estimate of CKA [42].

2.3 Experimental Setup

We provide a brief overview of our experimental setup here. All of our experiments were run on machines with either NVidia Titan RTX GPUs with 24GB of memory or RTX A4000 GPUs with 16GB of memory. Further details are in Appendix A.

Models and datasets. We consider three commonly used image datasets: CIFAR-10 [32], ImageNette [25], and ImageWoof [25], where the latter two are subsets of ImageNet [11], which we use due to the high cost of adversarial training on the full ImageNet dataset. We use the Wide Resnet [63] class of models on CIFAR-10 dataset and ImageNet-based ResNets for ImageNette and Imagewoof datasets.

Adversarial training. We follow standard convention with ℓ_∞ perturbations and use $\epsilon = \frac{8}{255}$ for CIFAR-10 and $\epsilon = \frac{4}{255}$ for ImageNet based datasets. We use 10-step projected gradient descent (PGD) attack during training and use 20 steps at test time to calculate adversarial representations.

Representation similarity. We will be using mainly using CKA to compare activation matrices derived from different benign or adversarial images. In online CKA, we use a batch-size of 1024 and take 3 passes over the dataset to reduce any stochasticity in the output similarity score. In layer-wise similarity analyses, we consider all layers, including convolutions, pooling, activation, and batch-normalization layers.

3 How do representations from robust and non-robust networks differ?

Robust training is expected to be a harder training objective than non-robust training, since it optimizes for both accuracy and robustness. The resulting trade-off is also reflected in final performance, where the benign accuracy of robust networks is much lower than non-robust networks [35]. In this section, we aim to understand the impact of robust training on internal representations, in particular by comparing benign representations in non-robust and robust networks. Further experiments and results from this section are included in Appendix B. We take the following two-fold approach:

1) Comparing characteristics: Absence of block structure. When comparing layerwise similarity in non-robust networks, numerous works have revealed a 'block structure', with high similarity between the layers comprising a block, and low similarity outside it [31, 42, 45] (Non-robust network plots in Figure 2).We observe that when moving from benign to robust training, while keeping

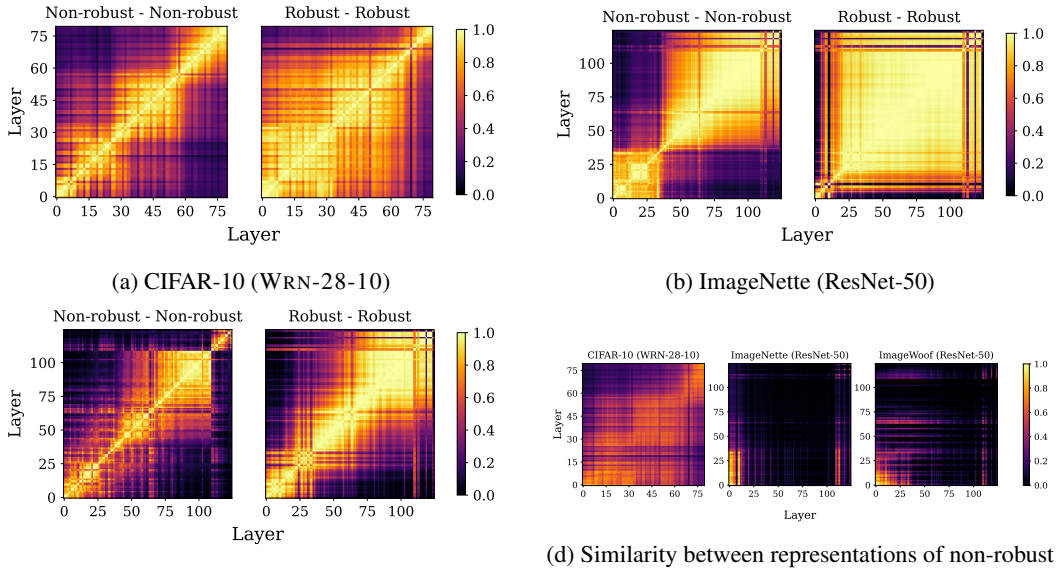

(a) CIFAR-10 (WRN-28-10)

(b) ImageNette (ResNet-50)

(c) ImageWoof (ResNet-50)

(d) Similarity between representations of non-robust and robust models.

Figure 2: **Stark differences in the cross-layer similarity and block structure for robust networks.** We measure the similarity of *benign representations* for three datasets across all pairs of layers in both non-robust and robust networks. *(a, b, c):* Robust networks have an amplified degree of cross-layer similarity, even at long-range, which diminishes the well known block structure characteristic observed in non-robust networks [42]. *(d)* We observe low similarity between representations of non-robust and robust models with identical experimental setups.

everything else constant, the *block structure significantly fades*. The much weaker block structure in robustly trained networks is accompanied by the presence of *long-range similarities* between layers, with layers having high similarity to those much farther away in the network (Figure 2).

2) Direct comparison: Poor similarity between non-robust and robust network representations. To further investigate the unique characteristics of robust networks, we conduct a cross-layer comparison of benign representations in non-robust and robust networks (Figure 2d). We find a very low degree of similarity across both network representations, which further shows that robust networks had indeed learned strikingly different representations than non-robust networks.

We also show that both of these observations generalize across architectures, datasets and threat models (see Appendix B). We now delve deeper into *analyzing cross-layer characteristics of robust networks representations.*

Impact of robust training strength. We investigate this disappearance of block structure in robustly trained networks further by varying both the adversarial budget (ϵ) used for training and the width of the network (Figure 3). As the training ϵ increases, the block structure becomes fainter, eventually disappearing entirely. The block structure is also impacted by network width, with it being marginally more pronounced in larger networks. However, this distinction is largely absent at larger values of ϵ. This establishes that increasing the value of ϵ is making the task more complex, so maintaining the same model capacity leads to a decrease in relative capacity (indicated by high similarity across representations). This conclusion relates to several findings in the adversarial robustness literature on the topic of low-rank representations. Encouraging low dimensionality of learned representations through regularization has been found to increase adversarial robustness [49, 34, 39]. While it is outside the scope of this work, it would be interesting for future work to study if the task of learning low-dimensional robust representations is inherently more complex, leading to higher utilization of model capacity and thereby reducing differentiation between layers.

Impact of architecture. Previously Nguyen et al. [42] observed that increasing network width, thus capacity, leads to emergence of block-structure in non-robust networks. Thus we incrementally increase the width of robust Wide-ResNet architecture on CIFAR-10 dataset and measure the cross-layer representation similarity of benign features (Figure 3). Even after increasing network capacity by an order of magnitude, we do not see significant variation in the characteristics of robust network

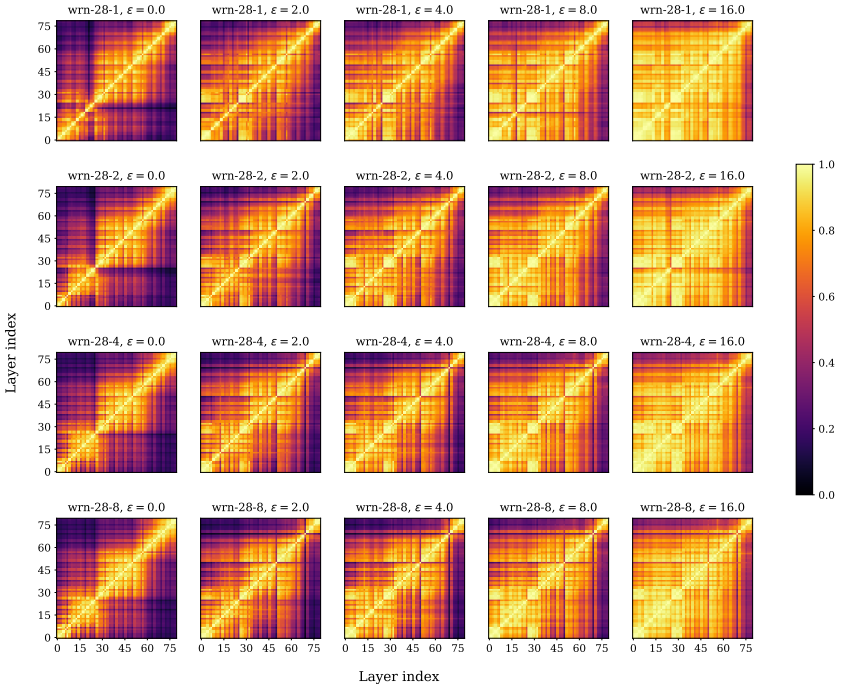

Figure 3: **Delving deeper into cross-layer similarity.** To better understand the unique cross-layer characteristics in benign representations of robust networks (Figure 2), we ablate along two main design choices: 1) Strength of adversarial attacks in robust training (by increasing perturbation budget (ϵ)) and 2) Changing network size (by increasing network width). We observe that increasing the strength of adversarial perturbations in training predominantly leads to amplification of cross-layer similarity, i.e., higher degree of brightness in the plots. Increasing network capacity, even by an order of magnitude, does not substantially change this phenomenon. We used Wide-ResNet architectures with the CIFAR-10 dataset for this experiment.

representations. These results suggest that increasing width in robust networks doesn't lead to a drastic shift in similarity of internal layer representations.

4 Probing the impact of adversarial perturbations on representations

Robust training aims to learn both high quality benign and robust representations. In the previous section we characterized the impact of robust training on benign representations. In this section, we focus on understanding the characteristics of adversarial representations in robust networks. Detailed results, as well as ablations over architecture and threat model, are in Appendix C. We first analyze how adversarial perturbations distort the internal representations as we go deeper into the network, *i.e.*, compare adversarial and benign representations. Next, we analyze whether the distortions introduced by adversarial perturbations can also provide insights into why such perturbations transfer between different networks.

4.1 Impact of adversarial perturbations across layers in non-robust and robust networks

In this experiment, we measure the CKA similarity between benign image representations and corresponding adversarial image representations.

Early layers are the least affected. Adversarial perturbations are crafted to corrupt final layer representations. In our experiments, as expected, the cross-layer similarity score decays to near zero by the final layer (Figure 4). However, we observe another surprising trend in which adversarial representations share a high degree of similarity with a fraction (up to one-third for ImageNette and Imagewoof datasets) of early layers. We find this observation holds across architectures and budgets, indicating that earlier layers representations, even in benign networks, are robust to adversarial perturbations.

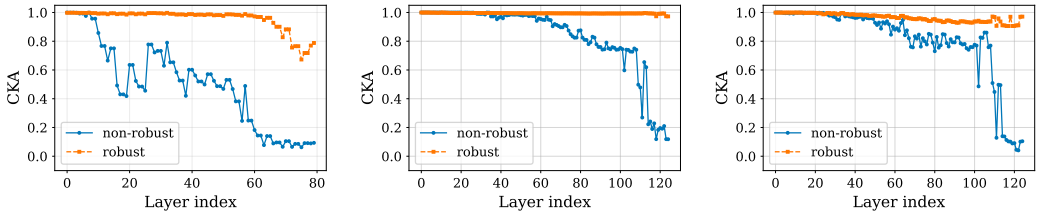

(a) CIFAR-10 (b) ImageNette (c) ImageWoof

Figure 4: **Divergence of adversarial representations from benign ones.** We observe how adversarial perturbations, which are known to heavily impact model output, distort the internal representations in comparison to non-adversarial representations. we compare adversarial representations from corresponding layers in non-robust and robust networks. As expected, adversarial and benign representations in non-robust networks display high dissimilarity by the end of network. Unexpectedly, such divergence is very small for a non-trivial fraction of early layers (up to one-third). Robust training successfully reduces the impact of adversarial perturbations, thus leading to similar benign and adversarial representations in robust networks.

Robust networks successfully prevent the distortion of internal representations. For robustly trained networks, benign and robust representations maintain a high degree of similarity throughout the network, with divergence only occurring in the last 10 layers or so. In our ablation on network size (Figure 20 in Appendix C), we see that increasing the size of the network leads to increased differentiation, implying sufficient capacity for increased separability between benign and perturbed representations.

4.2 Understanding transferability through the lens of internal representation similarity

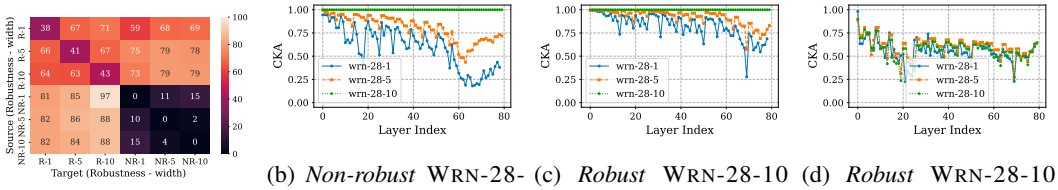

(a) Transfer accuracy of adversarial examples. (b) *Non-robust* WRN-28-10 vs. *non-robust* Wide Resnets. (c) *Robust* WRN-28-10 and other *robust* Wide Resnets. (d) *Robust* WRN-28-10 and other *non-robust* Wide Resnets

Figure 5: **Analyzing cross-architecture representations to understand similarity.** *(a)* Measuring the robust accuracy of adversarial examples transferred between robust (R) and non-robust (NR) Wide-ResNet networks of varying width (e.g., R-5 refers to Robust WRN-28-5). Low robust accuracy implies high transferability. *(b, c, d)* We measure CKA between source and target networks, where these representations are extracted using adversarial examples generated for the source network. When both networks are trained in the same fashion (benign or robust), the layer wise similarity is generally high at earlier layers but drops off towards the end. In contrast, it drops right after the first layer from robust to non-robust network, a set of networks which also have least transferability.

It is well-known that adversarial examples are *transferable* from one architecture to another, i.e., adversarial examples generated on one network achieve the misclassification objective on others too. In Figure 5a, we measure the transferability between non-robust and robust networks. Intriguingly, as previously validated by [7], transferability is higher among some networks (non-robust to non-robust) while much poorer for others (robust to non-robust). High transferability indicates that the target network has learned a similar decision boundary to the source network. We aim to better understand this phenomenon by comparing the internal representations of source and target networks. We first generate adversarial examples, and their corresponding internal layer representations, from a source network (WRN-28-10 in this case). We compare them with internal layer representations of these

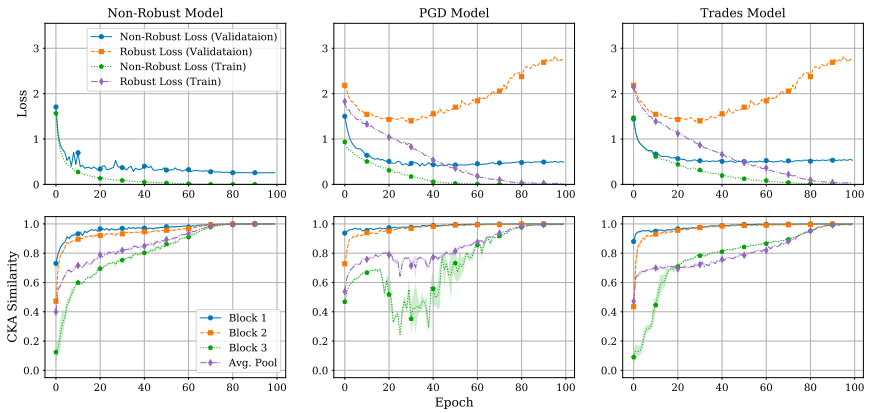

Figure 6: **Variation in convergence of different layers.** We compare representations from each epoch of training with the final learned representations of a network across both non-robust and robust (both PGD-based and TRADES) training techniques. We observe that representations obtained from the output of the first two blocks converge to their final state very early in the training process and have very little variation in both non-robust and robust network. We also find that later layers exhibit more complex behavior, with signs of overfitting when early stopping is not used, and a lack of stability from one epoch to the next. CKA values are averaged over three training runs with different random initializations.

adversarial examples on the target network. We consider transfer from non-robust to robust, robust to robust, and robust to non-robust networks [4] (Figure 5).

For transfer from non-robust to non-robust or robust-robust, where highest transferability occurs, we observe high degree of similarity between representations at early layers. It indicates that the transferred adversarial examples distort the internal representations in a similar fashion as source network. The most intriguing aspect in Figure 5a is extremely poor transferability from robust to non-robust networks. We establish that this is due to significant differences in representations where, even across identical architectures, we observe a large drop in CKA right after input layer. It shows that adversarial perturbations from robust nework distorts the internal representations of non-robust network in a strikingly different manner (even at very early layers), which likely renders them ineffective to cause an adversarial effect at the output of the network.

5 Evolution of internal representation dynamics during robust training

In this section, we track the evolution of representations learned by robust training methods over the course of training epochs in the optimization process. We study the following two convergence properties: 1) Rate of convergence at different layers, and 2) Stability of different layers throughout learning. As in earlier sections, we use CKA to measure similarity, but in this section we *compare the benign representations of the same layer across time*. We present our results for Wide-ResNet architecture in Figure 6, where we compare the representations at each epoch to the final epoch (epoch 100). We further investigate across architectures, layers, and attack budgets in Appendix D.

Early layers converge faster than later layers. Benign representations after the first two blocks of WRN-28-10 are highly similar to the representation obtained at the end of training, after just ten epochs (Figure 6). This is true for all the training methods considered. In Appendix D, we show this largely holds true across architectures and smaller budgets. Our observation relates to the intuition that early layers learn simpler features [33, 62, 64], thus are learned much faster than complex feature learned by later layers. Only with high budget (see $\epsilon = \frac{16}{255}$ in Fig. 26), i.e., stronger attacks, we observe a deviation from this trend where second block convergence is slower. We further validate this with layer-freezing experiments in Appendix D.5.

[4] Robust networks are known to be highly resilient to adversarial examples generated from non-robust networks (see Figure 5a).

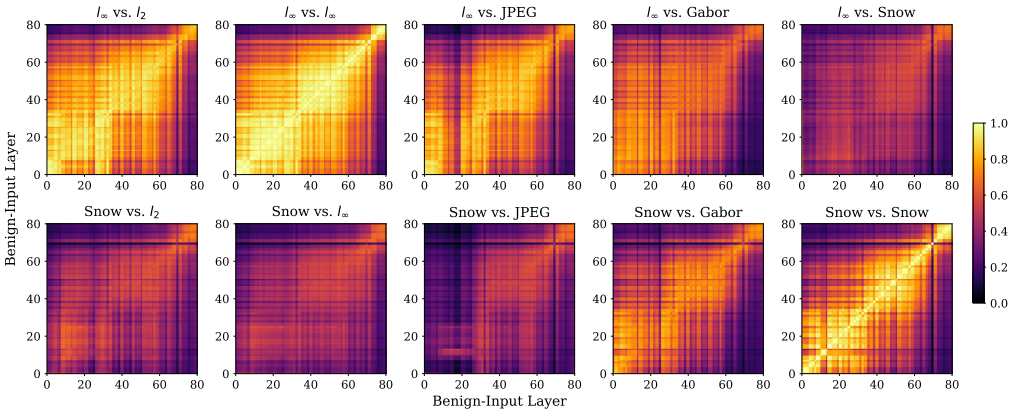

Figure 7: **Layer-wise similarity plots between different threat models**. The top row shows comparisons between all threat models and l_∞, and the second row shows comparisons between all threat models and Snow. The ℓ_p threat models are similar to each other across layers. Among the other threat models, Snow and Gabor display the highest similarity, which is surprising due to large differences in their visual representations.

Overfitting is predominantly visible in later layers. From the cross-epoch heatmap of similarities between adversarial representations (Figure 25), we observe that later layer representations only exhibit similarity off-diagonal at the beginning (until epoch 30) and end of training. This clearly shows that multiple local minima are found during training. This is true to a less pronounced degree for benign representations. In Fig. 6, we also observe the adversarial validation loss increasing after around 30 epochs, while the training loss keeps decreasing, indicating overfitting. After this point in training, the CKA similarity between drops with respect to both the epoch 30 and final representation drops significantly in later layers, while the earlier layers remain unaffected. This strongly indicates that the later layers have overfit to the training data. While it is already known that adversarial loss induces overfitting at the output layer [48], our results show that this degree of overfitting is not present in all layers of the network. This finding supports previous work which shows that retraining just the final layer of a deep network can greatly increase its robustness to spurious correlations in training data [29]. We hypothesize that a layer-by-layer analysis of overfitting in networks may be useful in fine-tuning robust networks.

Adversarial training reduces stability of internal representations during training. While subsequent epoch representations tend to be very similar to each other in non-robust training, there there can be very large jumps in similarity between one epoch and the next, indicating a less stable convergence. This effect further accentuates when training with a higher perturbation budget or when training a larger network (Appendix D).

6 How does the threat model impact representations?

Throughout the paper, we have focused on a single threat model: ℓ_∞ perturbations. In this section, we extend our analysis of robust representations to understand what exactly the link is between the visual similarity of threat models and the representations of models trained to be robust to them. To this end, we consider *four* additional threat models: ℓ_2, JPEG, Gabor and Snow [28] (visualized in Figure 8). We also examine the generalizability of our earlier results across these threat models. For space reasons, all associated figures from this section are in Appendix E.

Do visually similar attacks lead to similar robust representations? Representation similarity gives us a method by which we can compare how different classes of adversarial perturbations affect learned representations. Using CKA, we plotted the cross-layer similarity of robust WRN-28-10 networks adversarially trained against five different threat models (ℓ_2, ℓ_∞, JPEG, Gabor, and Snow) (Figure 7). These comparisons lend credence to conventional knowledge about these threat models. The layerwise similarity plot between l_2 and l_∞ robust models is strikingly similar to CKA plots between robust models trained on the same threat model. This mirrors theoretical results on correspondences

between ℓ_p threat models [55]. We also observe a higher average similarity when comparing an ℓ_∞ model with a JPEG model than with Snow or Gabor models. This makes intuitive sense, given the ℓ_∞ constraint inherent in the JPEG attack. When using CKA to compare against the Snow threat model, we observe that the highest average similarity is achieved with Gabor. This represents a novel insight into these threat classes, as correspondence between the two was not previously known, and may indicate the possibility of models jointly robust to these threat models.

Alignment of budgets across different attacks. CKA can also give insight into the varying effects of changing perturbation strengths within different threat models. Expanding on our experiments above (all figures are in Appendix E), we compared representations between different threat models while varying perturbation strengths. Between ℓ_∞ and Gabor models, the layerwise similarity structure is much more sensitive to changes in the strength used in ℓ_∞-robust training than in Gabor-robust training. For more closely related attacks, like ℓ_∞ and JPEG, we see similar degradations of the structure when changing the strength of either attack. Furthermore, the structure is largely preserved when the attack strengths are changed in tandem. These results may be useful for developing techniques for training models to be jointly-robust against different classes of attack.

Layerwise structure across threat models. We find that across all threat models except Snow, robust and benign activations exhibit high similarity (Figure 22). Changing budgets across the same threat model (Figure 30), we find that ℓ_p threat models' representations evolve more gradually.

7 Discussion

Limitations. The key limitations of our study arise from the fact that all discoveries are predicated on the effectiveness of the RS metric used to discern differences between representations. Further, the nature of our study can only unearth correlations between layer-wise and aggregate properties such as accuracy and loss. Establishing causal links needs further investigation, perhaps inspired by our findings as we discuss below. Finally, methods to improve robust training are beyond the scope of this paper. They need to be derived from a careful analysis of the observations in this paper for actionable changes to training strategies and architectures.

Future Work. Our observations highlight that robust networks could be improved in 3 key ways:

1. Staggered freezing of layers during training: Our results from § 5 indicate that early layers do not need to be updated post a few epochs of training, since their learned representations do not change much during training. Thus, knowledge of a network's training dynamics derived from CKA analysis can be used to increase the efficiency of training through the freezing of early layers.

2. Increasing layer-wise differentiation during training: Our results show there is a much greater degree of local similarity among learned representations for robust networks when compared to non-robust ones. This similarity also increases when the training budget is increased. We suspect this lack of layer-wise differentiation is part of the reason why robust networks do not achieve high accuracy on clean data. Using regularization methods that promote increased layer-wise differentiation during robust training may alleviate this issue, and is a compelling direction for future work.

3. Choosing threat models for joint robust training: Past work on training models jointly robust to multiple attacks has focused on different ℓ_p perturbations. We posit that our analysis of the similarity of representations obtained from different threat models can be utilized to determine sets of threat models for which joint robustness is possible, and if the model has sufficient capacity. Further, the layer-wise analysis can be used to add appropriate regularizers to ensure convergence, an issue exacerbated by the presence of multiple types of adversarial examples.

Acknowledgments and Disclosure of Funding

We thank our anonymous reviewers for their insightful feedback. CC, ANB, BYZ and HZ were supported in part by NSF grants CNS-1949650, CNS-1923778, CNS-1705042, the C3.ai DTI, and the DARPA GARD program. VS and PM were supported in part by NSF grants CNS-1553437 and CNS-1704105, the ARL's A2I2, the ONR Young Investigator Award, the ARO Young Investigator Prize, Schmidt DataX award, Princeton E-ffiliates Award, and Princeton Gordon Y. S. Wu Fellowship. Any opinions, findings, and conclusions or recommendations expressed in this material are those of the authors and do not necessarily reflect the views of any funding agencies.

References

[1] Andriushchenko, M. and Flammarion, N. (2020). Understanding and improving fast adversarial training. *Advances in Neural Information Processing Systems*, 33:16048–16059.

[2] Bansal, Y., Nakkiran, P., and Barak, B. (2021). Revisiting model stitching to compare neural representations. *Advances in Neural Information Processing Systems*, 34.

[3] Beal, J., Wu, H.-Y., Park, D. H., Zhai, A., and Kislyuk, D. (2022). Billion-scale pretraining with vision transformers for multi-task visual representations. In *Proceedings of the IEEE/CVF Winter Conference on Applications of Computer Vision*, pages 564–573.

[4] Biggio, B., Corona, I., Nelson, B., Rubinstein, B. I., Maiorca, D., Fumera, G., Giacinto, G., and Roli, F. (2014). Security evaluation of support vector machines in adversarial environments. In *Support Vector Machines Applications*, pages 105–153. Springer.

[5] Brown, T., Mann, B., Ryder, N., Subbiah, M., Kaplan, J. D., Dhariwal, P., Neelakantan, A., Shyam, P., Sastry, G., Askell, A., et al. (2020). Language models are few-shot learners. *Advances in neural information processing systems*, 33:1877–1901.

[6] Conneau, A., Khandelwal, K., Goyal, N., Chaudhary, V., Wenzek, G., Guzmán, F., Grave, E., Ott, M., Zettlemoyer, L., and Stoyanov, V. (2019). Unsupervised cross-lingual representation learning at scale. *arXiv preprint arXiv:1911.02116*.

[7] Croce, F., Andriushchenko, M., Sehwag, V., Debenedetti, E., Flammarion, N., Chiang, M., Mittal, P., and Hein, M. (2020). Robustbench: a standardized adversarial robustness benchmark. *arXiv preprint arXiv:2010.09670*.

[8] Croce, F. and Hein, M. (2021). Adversarial robustness against multiple l_p-threat models at the price of one and how to quickly fine-tune robust models to another threat model. *arXiv:2105.12508 [cs]*.

[9] Csiszárik, A., Kőrösi-Szabó, P., Matszangosz, Á., Papp, G., and Varga, D. (2021). Similarity and matching of neural network representations. *Advances in Neural Information Processing Systems*, 34.

[10] Deng, J., Dong, W., Socher, R., Li, L.-J., Li, K., and Fei-Fei, L. (2009a). ImageNet: A Large-Scale Hierarchical Image Database. In *CVPR09*.

[11] Deng, J., Dong, W., Socher, R., Li, L.-J., Li, K., and Fei-Fei, L. (2009b). Imagenet: A large-scale hierarchical image database. In *2009 IEEE conference on computer vision and pattern recognition*, pages 248–255. Ieee.

[12] Deng, J., Guo, J., Xue, N., and Zafeiriou, S. (2019). Arcface: Additive angular margin loss for deep face recognition. In *Proceedings of the IEEE/CVF conference on computer vision and pattern recognition*, pages 4690–4699.

[13] Devlin, J., Chang, M.-W., Lee, K., and Toutanova, K. (2018). Bert: Pre-training of deep bidirectional transformers for language understanding. *arXiv preprint arXiv:1810.04805*.

[14] Ding, F., Denain, J.-S., and Steinhardt, J. (2021). Grounding representation similarity through statistical testing. *Advances in Neural Information Processing Systems*, 34.

[15] Dosovitskiy, A., Beyer, L., Kolesnikov, A., Weissenborn, D., Zhai, X., Unterthiner, T., Dehghani, M., Minderer, M., Heigold, G., Gelly, S., Uszkoreit, J., and Houlsby, N. (2021). An image is worth 16x16 words: Transformers for image recognition at scale. In *International Conference on Learning Representations*.

[16] Dwivedi, K., Huang, J., Cichy, R. M., and Roig, G. (2020). Duality diagram similarity: a generic framework for initialization selection in task transfer learning. In *European Conference on Computer Vision*, pages 497–513. Springer.

[17] Gao, R., Cai, T., Li, H., Hsieh, C.-J., Wang, L., and Lee, J. D. (2019). Convergence of adversarial training in overparametrized neural networks. *Advances in Neural Information Processing Systems*, 32.

[18] Gavrikov, P. and Keuper, J. (2022). Adversarial robustness through the lens of convolutional filters. *arXiv preprint arXiv:2204.02481*.

[19] Gilboa, D. and Gur-Ari, G. (2019). Wider networks learn better features. *arXiv preprint arXiv:1909.11572*.

[20] Gowal, S., Qin, C., Uesato, J., Mann, T., and Kohli, P. (2020). Uncovering the limits of adversarial training against norm-bounded adversarial examples. *arXiv preprint arXiv:2010.03593*.

[21] Grigg, T. G., Busbridge, D., Ramapuram, J., and Webb, R. (2021). Do self-supervised and supervised methods learn similar visual representations? *arXiv preprint arXiv:2110.00528*.

[22] Hardoon, D. R., Szedmak, S., and Shawe-Taylor, J. (2004). Canonical correlation analysis: An overview with application to learning methods. *Neural computation*.

[23] Hendrycks, D. and Dietterich, T. (2018). Benchmarking neural network robustness to common corruptions and perturbations. In *International Conference on Learning Representations*.

[24] Hinton, G., Deng, L., Yu, D., Dahl, G. E., Mohamed, A.-r., Jaitly, N., Senior, A., Vanhoucke, V., Nguyen, P., Sainath, T. N., et al. (2012). Deep neural networks for acoustic modeling in speech recognition: The shared views of four research groups. *IEEE Signal processing magazine*, 29(6):82–97.

[25] Howard, J. (2020). imagenette. `https://github.com/fastai/imagenette`.

[26] Huang, H., Wang, Y., Erfani, S., Gu, Q., Bailey, J., and Ma, X. (2021). Exploring architectural ingredients of adversarially robust deep neural networks. *Advances in Neural Information Processing Systems*, 34.

[27] Ilyas, A., Santurkar, S., Tsipras, D., Engstrom, L., Tran, B., and Madry, A. (2019). Adversarial examples are not bugs, they are features. *Advances in neural information processing systems*, 32.

[28] Kang, D., Sun, Y., Hendrycks, D., Brown, T., and Steinhardt, J. (2019). Testing robustness against unforeseen adversaries. *arXiv preprint arXiv:1908.08016*.

[29] Kirichenko, P., Izmailov, P., and Wilson, A. G. (2022). Last layer re-training is sufficient for robustness to spurious correlations. *arXiv preprint arXiv:2204.02937*.

[30] Kornblith, S., Chen, T., Lee, H., and Norouzi, M. (2021). Why do better loss functions lead to less transferable features? *Advances in Neural Information Processing Systems*, 34.

[31] Kornblith, S., Norouzi, M., Lee, H., and Hinton, G. (2019). Similarity of neural network representations revisited. In *International Conference on Machine Learning*, pages 3519–3529. PMLR.

[32] Krizhevsky, A., Hinton, G., et al. (2009). Learning multiple layers of features from tiny images.

[33] Krizhevsky, A., Sutskever, I., and Hinton, G. E. (2012). Imagenet classification with deep convolutional neural networks. *Advances in neural information processing systems*, 25.

[34] Leavitt, M. L. and Morcos, A. (2020). Linking average-and worst-case perturbation robustness via class selectivity and dimensionality. *arXiv preprint arXiv:2010.07693*.

[35] Madry, A., Makelov, A., Schmidt, L., Tsipras, D., and Vladu, A. (2018). Towards deep learning models resistant to adversarial attacks. In *ICLR*.

[36] Mahajan, D., Girshick, R., Ramanathan, V., He, K., Paluri, M., Li, Y., Bharambe, A., and Van Der Maaten, L. (2018). Exploring the limits of weakly supervised pretraining. In *Proceedings of the European conference on computer vision (ECCV)*, pages 181–196.

[37] Morcos, A., Raghu, M., and Bengio, S. (2018). Insights on representational similarity in neural networks with canonical correlation. *Advances in Neural Information Processing Systems*, 31.

[38] Nakkiran, P. (2019). Adversarial robustness may be at odds with simplicity. *arXiv preprint arXiv:1901.00532*.

[39] Nayebi, A. and Ganguli, S. (2017). Biologically inspired protection of deep networks from adversarial attacks. *arXiv preprint arXiv:1703.09202*.

[40] Neyshabur, B., Sedghi, H., and Zhang, C. (2020). What is being transferred in transfer learning? *Advances in neural information processing systems*, 33:512–523.

[41] Nguyen, Q. and Hein, M. (2018). Optimization landscape and expressivity of deep cnns. In *International conference on machine learning*, pages 3730–3739. PMLR.

[42] Nguyen, T., Raghu, M., and Kornblith, S. (2020). Do wide and deep networks learn the same things? uncovering how neural network representations vary with width and depth. *arXiv preprint arXiv:2010.15327*.

[43] Raghu, A., Raghu, M., Bengio, S., and Vinyals, O. (2020). Rapid learning or feature reuse? towards understanding the effectiveness of maml. In *International Conference on Learning Representations*.

[44] Raghu, M., Gilmer, J., Yosinski, J., and Sohl-Dickstein, J. (2017). Svcca: Singular vector canonical correlation analysis for deep learning dynamics and interpretability. *Advances in neural information processing systems*, 30.

[45] Raghu, M., Unterthiner, T., Kornblith, S., Zhang, C., and Dosovitskiy, A. (2021). Do vision transformers see like convolutional neural networks? *Advances in Neural Information Processing Systems*, 34.

[46] Raghunathan, A., Steinhardt, J., and Liang, P. (2018). Certified defenses against adversarial examples. In *International Conference on Learning Representations*.

[47] Ribeiro, M. T., Singh, S., and Guestrin, C. (2016). " why should i trust you?" explaining the predictions of any classifier. In *Proceedings of the 22nd ACM SIGKDD international conference on knowledge discovery and data mining*, pages 1135–1144.

[48] Rice, L., Wong, E., and Kolter, Z. (2020). Overfitting in adversarially robust deep learning. In *International Conference on Machine Learning*, pages 8093–8104. PMLR.

[49] Sanyal, A., Kanade, V., Torr, P. H., and Dokania, P. K. (2018). Robustness via deep low-rank representations. *arXiv preprint arXiv:1804.07090*.

[50] Selvaraju, R. R., Cogswell, M., Das, A., Vedantam, R., Parikh, D., and Batra, D. (2017). Grad-cam: Visual explanations from deep networks via gradient-based localization. In *Proceedings of the IEEE international conference on computer vision*, pages 618–626.

[51] Shen, J., Pang, R., Weiss, R. J., Schuster, M., Jaitly, N., Yang, Z., Chen, Z., Zhang, Y., Wang, Y., Skerrv-Ryan, R., et al. (2018). Natural tts synthesis by conditioning wavenet on mel spectrogram predictions. In *2018 IEEE international conference on acoustics, speech and signal processing (ICASSP)*, pages 4779–4783. IEEE.

[52] Simonyan, K., Vedaldi, A., and Zisserman, A. (2013). Deep inside convolutional networks: Visualising image classification models and saliency maps. *arXiv preprint arXiv:1312.6034*.

[53] Sundararajan, M., Taly, A., and Yan, Q. (2017). Axiomatic attribution for deep networks. In *International conference on machine learning*, pages 3319–3328. PMLR.

[54] Szegedy, C., Zaremba, W., Sutskever, I., Bruna, J., Erhan, D., Goodfellow, I., and Fergus, R. (2013). Intriguing properties of neural networks. *arXiv preprint arXiv:1312.6199*.

[55] Tramèr, F. and Boneh, D. (2019). Adversarial training and robustness for multiple perturbations. In *Advances in Neural Information Processing Systems*, pages 5866–5876.

[56] Tsipras, D., Santurkar, S., Engstrom, L., Turner, A., and Madry, A. (2018). Robustness may be at odds with accuracy. *arXiv preprint arXiv:1805.12152*.

[57] Vaswani, A., Shazeer, N., Parmar, N., Uszkoreit, J., Jones, L., Gomez, A. N., Kaiser, Ł., and Polosukhin, I. (2017). Attention is all you need. *Advances in neural information processing systems*, 30.

[58] Vulić, I., Ponti, E. M., Litschko, R., Glavaš, G., and Korhonen, A. (2020). Probing pretrained language models for lexical semantics. In *Proceedings of the 2020 Conference on Empirical Methods in Natural Language Processing (EMNLP)*, pages 7222–7240, Online. Association for Computational Linguistics.

[59] Wong, E., Santurkar, S., and Madry, A. (2021). Leveraging sparse linear layers for debuggable deep networks. In *International Conference on Machine Learning*, pages 11205–11216. PMLR.

[60] Xie, C. and Yuille, A. (2020). Intriguing properties of adversarial training at scale. In *ICLR*. arXiv: 1906.03787.

[61] Yang, Y., Hodgkinson, L., Theisen, R., Zou, J., Gonzalez, J. E., Ramchandran, K., and Mahoney, M. W. (2021). Taxonomizing local versus global structure in neural network loss landscapes. *Advances in Neural Information Processing Systems*, 34.

[62] Yosinski, J., Clune, J., Nguyen, A., Fuchs, T., and Lipson, H. (2015). Understanding neural networks through deep visualization. *arXiv preprint arXiv:1506.06579*.

[63] Zagoruyko, S. and Komodakis, N. (2016). Wide residual networks. *arXiv preprint arXiv:1605.07146*.

[64] Zeiler, M. D. and Fergus, R. (2014). Visualizing and understanding convolutional networks. In *European conference on computer vision*, pages 818–833. Springer.

[65] Zhang, H., Yu, Y., Jiao, J., Xing, E., El Ghaoui, L., and Jordan, M. (2019). Theoretically principled trade-off between robustness and accuracy. In *International conference on machine learning*, pages 7472–7482. PMLR.

[66] Zhou, J., Cui, G., Hu, S., Zhang, Z., Yang, C., Liu, Z., Wang, L., Li, C., and Sun, M. (2020). Graph neural networks: A review of methods and applications. *AI Open*, 1:57–81.

Checklist

1. For all authors...
   (a) Do the main claims made in the abstract and introduction accurately reflect the paper's contributions and scope? [Yes] See Section 3, 4, 5, 6
   (b) Did you describe the limitations of your work? [Yes] See Section 7
   (c) Did you discuss any potential negative societal impacts of your work? [N/A] Our paper is of an abstract nature and is quite removed from direct societal impact.
   (d) Have you read the ethics review guidelines and ensured that your paper conforms to them? [Yes] Having read the guidelines, given the abstract nature of the paper and the use of publicly available datasets, we do not foresee any ethical concerns from the publication of this paper.
2. If you are including theoretical results...
   (a) Did you state the full set of assumptions of all theoretical results? [N/A] All claims in the paper are of an empirical nature
   (b) Did you include complete proofs of all theoretical results? [N/A] See above
3. If you ran experiments...
   (a) Did you include the code, data, and instructions needed to reproduce the main experimental results (either in the supplemental material or as a URL)? [Yes] Code to reproduce all figures and results is included in the supplemental material
   (b) Did you specify all the training details (e.g., data splits, hyperparameters, how they were chosen)? [Yes] The baseline setup is in Section 2 and each section including the Appendix contains additional details as necessary.
   (c) Did you report error bars (e.g., with respect to the random seed after running experiments multiple times)? [No] Our results are averaged over 3 runs with the variation being too small to appear on our plots.

(d) Did you include the total amount of compute and the type of resources used (e.g., type of GPUs, internal cluster, or cloud provider)? [Yes] Section 2 contains compute details

4. If you are using existing assets (e.g., code, data, models) or curating/releasing new assets...
   (a) If your work uses existing assets, did you cite the creators? [Yes] Citations are included throughout the paper as appropriate
   (b) Did you mention the license of the assets? [N/A]
   (c) Did you include any new assets either in the supplemental material or as a URL? [No] All included assets are publicly available.
   (d) Did you discuss whether and how consent was obtained from people whose data you're using/curating? [N/A] See above
   (e) Did you discuss whether the data you are using/curating contains personally identifiable information or offensive content? [N/A] See above

5. If you used crowdsourcing or conducted research with human subjects...
   (a) Did you include the full text of instructions given to participants and screenshots, if applicable? [N/A]
   (b) Did you describe any potential participant risks, with links to Institutional Review Board (IRB) approvals, if applicable? [N/A]
   (c) Did you include the estimated hourly wage paid to participants and the total amount spent on participant compensation? [N/A]

In this Appendix, we aim to further validate the discoveries from the main body of the paper by conducting additional experiments. Our main focus is to ablate across architectures, representation similarity metrics and threat models to understand the generalizability of the results presented in the main body. For specific experiments, we also vary other parameters such as datasets as necessary.

The Appendix is organized as follows:

1. Further background and related work (Section A)
2. Exploring benign representations from robust networks (Section B)
3. Analysis of adversarially perturbed representations (Section C)
4. Impact of training parameters on layer-wise convergence (Section D)
5. Alignment of different threat models (Section E)

A Additional background and setup details

A.1 Representation similarity metrics

Canonical Correlation Analysis (CCA): Given activation matrices $X \in \mathbb{R}^{n \times p_1}, Y \in \mathbb{R}^{n \times p_2}$, canonical correlation analysis involves finding the orthogonal bases w_X^i, w_Y^i such that, after the matrices are projected onto their respective bases, correlation between the matrices is maximized [31]. The relevant summary statistic for CCA is $\bar{\rho}_{CCA}$, which is defined to be the mean of the canonical correlation coefficients ρ_i, for $1 \leq i \leq p_1$. ρ_i can be computed by

$$\begin{aligned} \rho_i = \max_{w_X^i, w_Y^i} \ & \text{corr}(Xw_X^i, Yw_Y^i) \\ s.t. \quad & \forall_{j<i} Xw_X^i \perp Xw_X^j \\ & \forall_{j<i} Yw_Y^i \perp Yw_Y^j \end{aligned} \tag{4}$$

In order to improve the robustness of CCA, **Singular Vector Canonical Correlation Analysis (SVCCA)** has been proposed by Raghu et al. [44]. Rather than compute CCA on X and Y, SVCCA first computes the singular vector decomposition of X and Y to find representations X' and Y' whose principle components explain a fixed proportion of the variance of X and Y. Standard CCA is then performed on X' and Y'.

Orthogonal Procrustes: The solution to the Orthogonal Procrustes problem is the left rotation of X that minimizes the Frobenius norm between the rotated X and Y. Formally, the problem is defined as

$$\min_R \|Y - RX\|_F^2, \ s.t. \ R^\intercal R = I \tag{5}$$

The Orthogonal Procrustes distance between X and Y is defined as

$$d_{\text{Proc}}(X, Y) = \|X\|_F^2 + \|Y\|_F^2 - 2\|X^\intercal Y\|_*, \tag{6}$$

where $\|\cdot\|_*$ is the nuclear norm [14]. When X and Y are normalized, this distance metric lies in the range $[0, 2]$. For our purposes, we compute the Orthogonal Procrustes similarity between normalized matrices X and Y, defined to be

$$S_{\text{Proc}}(X, Y) = 2 - d_{\text{Proc}}(X, Y) \tag{7}$$

A.2 Threat models

Most of our robust models were trained and evaluated on ℓ_∞ adversarial images. To supplement our results, we also ran experiments using conventional ℓ_2 attacks, as well as three adversarial attacks introduced by Kang et al. [28]: JPEG, Snow, and Gabor. The JPEG attack adds ℓ_p bounded adversarial noise to the JPEG-encoded space of images, rather than the pixel space of images. The Snow attack adds adversarially optimized visual occlusions to images that simulate snowfall. The Gabor attack optimizes the parameters of a Gabor kernel that is used to noise the image. Visual examples of these attacks are shown in Figure 8. Unless otherwise noted, for our CIFAR-10 experiments we run the ℓ_2 attack with $\epsilon = 1$, the JPEG attack with $\epsilon = 25$, the Snow attack with $\epsilon = 2$, and the Gabor attack with $\epsilon = 75$.

Figure 8: Adversarial examples generated by the threat models used in this paper.

	Benign Images		Adversarial Images	
Threat Model	Train Accuracy	Val. Accuracy	Train Accuracy	Val. Accuracy
Base	100.00	94.92	-	-
ℓ_∞ ($\epsilon = \frac{8}{255}$)	100.00	86.36	99.03	46.34
ℓ_2 ($\epsilon = 1$)	100.00	86.49	99.40	45.76
JPEG ($\epsilon = 25$)	100.00	84.65	91.98	45.52
Gabor ($\epsilon = 75$)	100.00	93.12	99.83	92.47
Snow ($\epsilon = 2$)	100.00	90.23	95.72	67.35

Table 2: Training and validation accuracies of the WRN-28-10 models used in this paper's experiments. The threat model represents the attack that each model was trained to be robust against, and adversarial images were generated using the same threat model and attack strength as was used in training.

A.3 Related Work

Tools to probe neural networks. These can be sorted broadly into two categories: i) *sample-based* and ii) *distribution-based* tools. Sample-based tools include techniques like input saliency maps [52], Grad-CAM [50], integrated gradients [53] etc. which are focused on interpreting the output of neural networks for specific inputs. On the other hand, loss surface visualizations [62, 41, 61] and representation similarity metrics [16, 31, 2, 44, 9] consider aggregate network properties derived from a set of samples.

Visualizing and validating network properties: Gilboa and Gur-Ari [19] use activation atlases to argue that the learned representations of wider networks are 'more informative' than shallower ones. To validate this assertion, they fine-tune a linear layer for a new task and find the wider representations perform better. Raghu et al. [45] study how transformers and CNNs learn features differently, Grigg et al. [21] analyze the differences between supervised and self-supservised representations and Kornblith et al. [30] consider the link between loss functions and feature transfer. Gavrikov and

	Non-Robust Model		ℓ_∞-Robust Model			
	Benign Images		Benign Images		Adversarial Images	
Width	Train Acc.	Val. Acc.	Train Acc.	Val. Acc.	Train Acc.	Val. Acc.
1	99.68	91.23	89.21	82.39	50.90	42.92
2	99.97	93.44	97.73	84.91	66.91	44.02
3	99.99	94.18	99.72	85.53	80.78	43.74
4	100.00	94.33	99.98	85.46	89.64	44.13
5	100.00	94.66	100.00	85.97	93.42	45.38
6	100.00	94.86	100.00	86.40	95.79	45.70
7	100.00	94.59	100.00	86.87	97.38	46.79
8	100.00	94.50	100.00	86.90	98.24	47.15
9	100.00	94.98	100.00	87.39	98.68	48.11
10	100.00	94.92	100.00	87.59	98.90	48.89

Table 3: Training and validation accuracies of the WRN-28-N models used in this paper's experiments, where N is the width factor. Robust models were trained on the ℓ_∞ threat model with $\epsilon = \frac{8}{255}$.

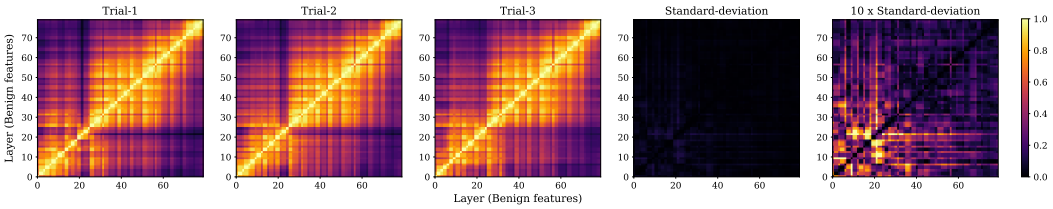

(a) Non-robust (WRN-28-1)

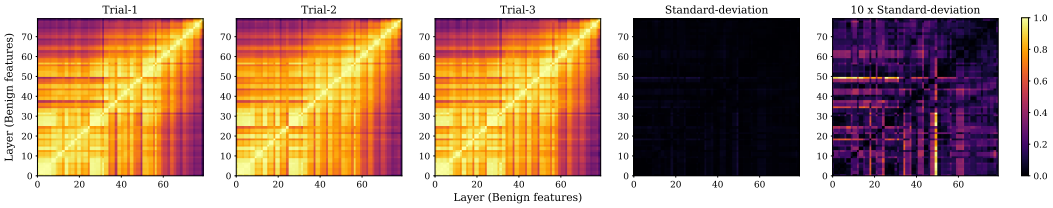

(b) Robust (WRN-28-1)

Figure 9: **Standard deviation of CKA across different random initializations.** We evaluate the CKA of three random initializations of non-robust and robust WRN-28-1 models, independently, and report the standard deviation. As shown above, the standard deviation is small, verifying that CKA is largely invariant to the random initialization of a network.

Keuper [18] use convolutional filters to understand the impact of robust training while Ilyas et al. [27] visualize what input features are needed for robust training.

A.4 Stability of CKA over different random initializations

Prior work has shown that CKA results are consistent across different random initializations [31]. We validate this by reporting the standard deviation of a cross-layer CKA computation in Figures 9a and 9b.

A.5 Stability of Online CKA over identically-trained networks

In Figures 10a and 10b, we show that the standard deviation of the unbiased estimate of CKA provided by our online CKA algorithm is very small.

B How are benign representations from robust networks different?

In this section, we provide additional details on how the benign representations from robustly trained networks differ from those obtained from non-robust networks (see §3 of the main paper). We ablate across RS metrics (appendix B.1), datasets (appendix B.2), robust training methods (appendix B.3) and architectures (appendix B.4). We also delve deeper into the link between RS metrics and classification accuracy in appendix B.7.

B.1 Using other representation similarity metrics

In Figure 11, we plot the layerwise similarity between the layers for benign representations from both a non-robust and robust model. Due to computational constraints when computing SVCCA and Orthogonal Procrustes, comparisons are shown using ResNet18 models, instead of the Wide ResNet models used throughout much of the rest of the paper. We note that the trend we observe of increased cross-layer similarity for robustly trained networks appears regardless of the RS metric used. Further, CKA leads to the most visually distinct structure. The broad takeaways from the different RS metrics are aligned enough that we focus on CKA for the remainder of the results in this Appendix.

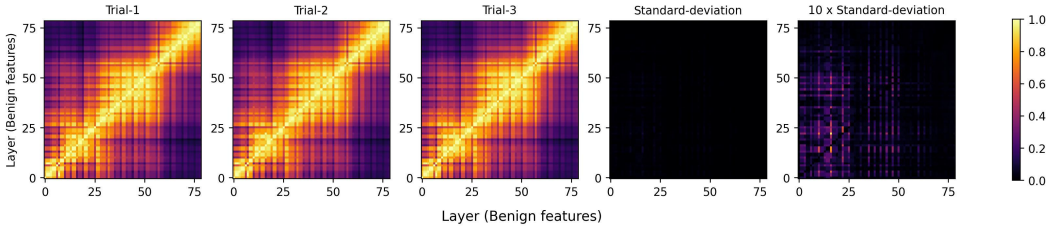

(a) Non-robust (WRN-28-10)

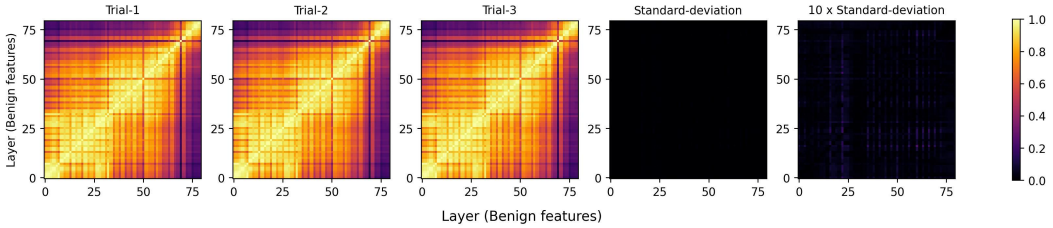

(b) Robust (WRN-28-10)

Figure 10: **Standard deviation of online CKA.** We evaluate the *online* CKA of a non-robust and robust WRN-28-10 model three times, independently, and report the standard deviation. As shown above, the standard deviation is very small, indicating that the insights from CKA are stable across individual evaluations.

B.2 Using other datasets

In Figures 12 and 13, we plot the layerwise similarities using CKA for ResNets trained on the ImageNette and Imagewoof datasets, both of which are subsets of the Imagenet dataset. These expand upon the results from Figure 2 of the main body, and show the stark differences between the representations obtained from non-robust and robust networks. The cross-layer similarities are far more pronounced for robust networks across datasets and architectures.

B.3 Comparing across robust training methods

In Fig. 14, we compare the benign representations from models robustly trained using two different robust training techniques: PGD-based adversarial training and TRADES. Both methods lead to very similar robust representations, and exhibit the same long-range similarity across layers.

In Figure 15, we compute cross-layer CKA similarities of seven robust networks from the RobustBench leaderboard. We find that, across training algorithms and architecture, these networks all display the lack of block structure that we saw in our own PGD-trained robust models.

B.4 Comparing across architectures

Recent work [26] has studied the influence of depth and width on adversarial robustness. We extend this investigation by comparing the benign representations obtained from Wide-ResNet models trained with different widths in Figure 16 with both non-robust and robust training. A few key observations stand out: i) early layers in different blocks are very similar across different widths for robust training, as compared to benign training, ii) increasing width only leads to large variations in learned representations in the last block for robust training, and iii) benign networks of different widths are similar deeper in the network, and different early on, with the opposite trend for robust networks. These results, taken together suggest that increased width early on in the network may not be particularly useful, but deeper in the network, leads to divergent representations, which can be investigated further to synthesize robust architectures.

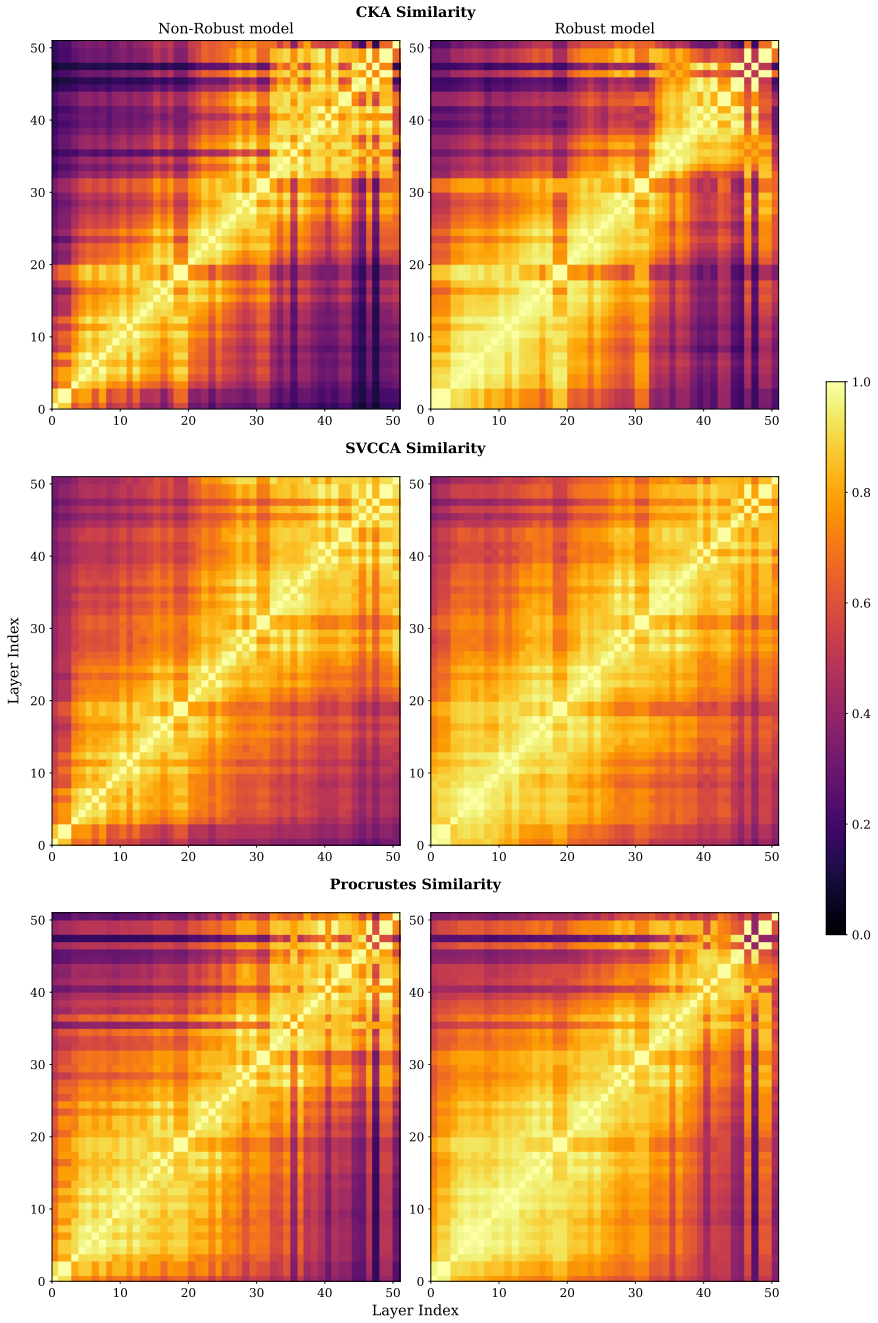

Figure 11: **Layerwise similarity plots of non-robust and robust ResNet18 models**. 3 different RS metrics are used: CKA, SVCCA, and Orthogonal Procrustes similarity over benign representations.

B.5 Comparing across attacks

In Figure 17, we compute cross-layer CKA similarity for benign and robust models using three different adversarial attack algorithms (Fast Gradient Sign Method, Projected Gradient Descent, and Auto-Projected Gradient Descent). Our results indicate that choice of attack causes little change in cross-layer similarity, with any differences likely being due to the relative strength of each attack.

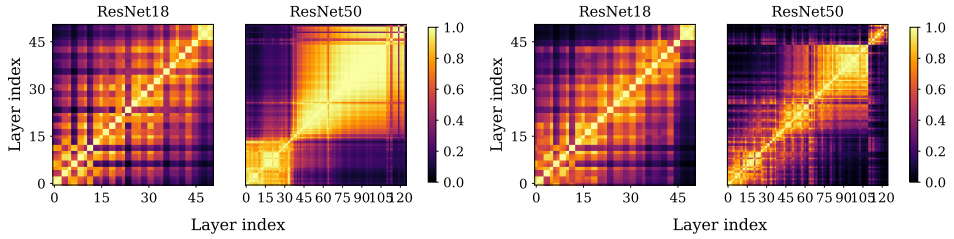

(a) ImageNette (Easy) (b) ImageWoof (Hard)

Figure 12: Cross layer CKA for *non-robust* network (using benign features)

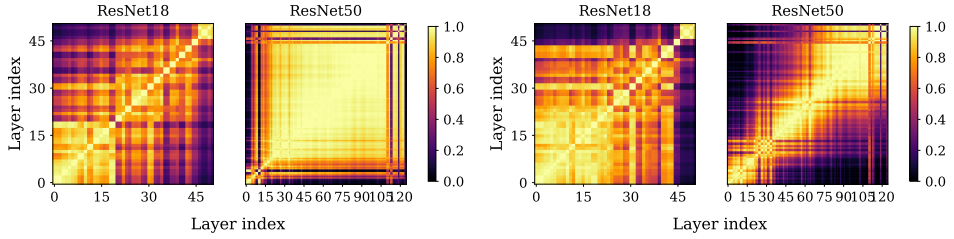

(a) ImageNette (Easy) (b) ImageWoof (Hard)

Figure 13: Cross layer CKA for *robust* network (using benign features)

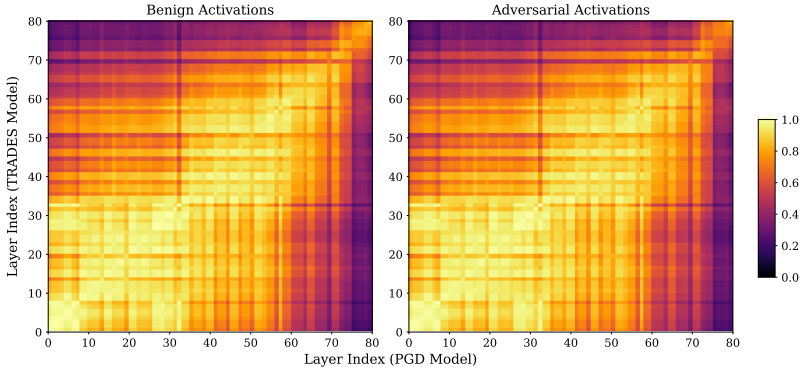

Figure 14: **PGD-based adversarial training and TRADES produce similar final representations.** Layerwise similarity between benign activations of a TRADES-trained WRN-28-5 model and a PGD-trained WRN-28-5 model.

B.6 Common Image Corruptions

Beyond adversarial perturbations, our methodology can also extend to other types of image perturbations. Results from networks trained to be robust to common types of non-adversarial corruptions are included in Figure 18. We find that these corruptions have a much less pronounced effect on learned representations than adversarial perturbations.

B.7 Delving deeper into CKA

Class-aware representation similarity. Standard RS metrics don't consider data labels, thus similarity scores doesn't provide insights in how individual class data impacts it. As an example, we consider Linear CKA (Equation 3 from the main body), where the similarity is dependent on the dot-product of vectorized Gram matrices ($\boldsymbol{K}, \boldsymbol{L}$). Two factors contribute to the similarity of gram matrices: 1) Intra-class similarity (C_1): $\sum_{i,j,y_i=y_j} K_{ij}L_{ij}$, 2) Inter-class similarity (C_2): $\sum_{i,j,y_i\neq y_j} K_{ij}L_{ij}$. When measured between identical features, linear CKA is 1, i.e., $C_1/(C_1 +$

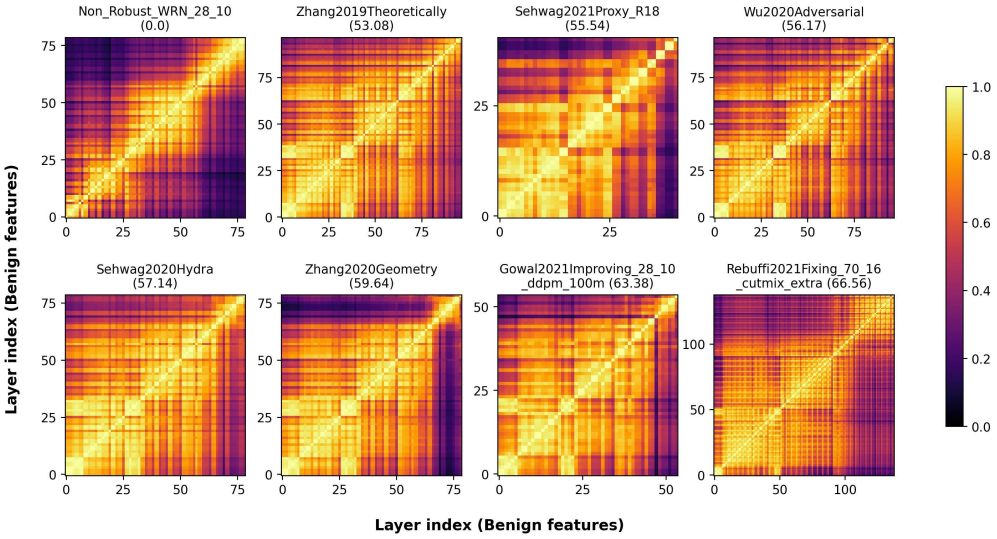

Figure 15: **Impact of adversarial training techniques (training algorithms, network architecture, and extra data) on our findings.**. Adversarial training performance has significantly improved over the last couple of years, where factors like better adversarial training techniques, better architectures, and extra training data helped. Our goal is to investigate whether our findings remain agnostic to these choices. We consider seven robust networks from the RobustBench leaderboard, which have varying performance and training setups. In each, we measure the cross-layer similarity of benign image features and find that the most robust networks do exhibit strikingly different cross-layer similarities than a non-robust network. Even when the network capacity is increased by an order of magnitude (e.g, in WRN-70-16), robust networks don't show as striking a block structure as a non-robust network. Each figure title corresponds to its key in the RobustBench leaderboard and the value in the title corresponds to the network robust accuracy on the CIFAR-10 dataset.

$C_2) + C_2/(C_1 + C_2)$. Under a near uniform distribution of class labels, only a small fraction of entries in gram matrices contribute to intra-class similarity (C_1), as there are a lot more cross terms in the CKA computation. However, when experimentally measuring the influence of both terms, i.e., we find that the contribution of intra-class CKA is very high, and it increases as we go deeper into the network. This is likely because separability of feature improves deeper in the network with similar class features being clustered together, which naturally increases the magnitude of C_1 in the similarity score.

We hypothesized that robust networks would have lower intra-class similarity as compared to non-robust networks, which would explain their lower classification accuracy on benign data. While this holds for the CIFAR-10 and ImageNette, for Imagewoof, robust networks have a much higher intra-class contribution. We leave a detailed investigation for future work.

C Adversarially Perturbed Representations

In this section, we add further results to back up the insights about the impact of adversarially perturbed data on resulting representations from §4.

C.1 Comparing benign and perturbed representations

In Figure 20, we can see, across, architectures, benign and perturbed representations differ at all layers except the first few for non-robust networks. In addition, for robustly trained networks, increasing width increases the divergence between benign and perturbed representations. This may indicate the presence of increased capacity to learn different representations for benign and adversarial inputs.

Across different threat models (Figure 22), we find robustly trained networks learn aligned benign and perturbed representations. This indicates that, in general, for most threat models, robust training

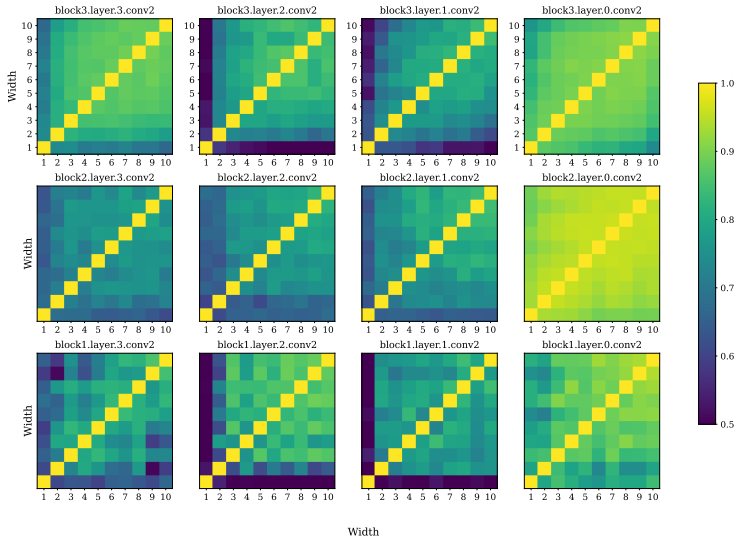

(a) *Non-robust* networks. Features extracted over *benign* images.

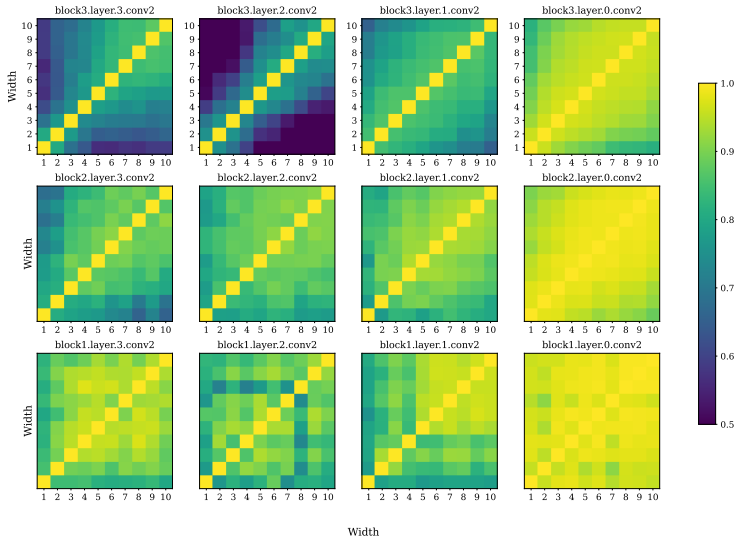

(b) *Robust* networks. Features extracted over *benign* images.

Figure 16: **Cross-model CKA between Wide ResNet models of different widths**. Data is presented across 12 convolutional layers, starting from the last convolutional layer, i.e., block3.layer3.conv2 and moving backward in the network. Robust networks have a high degree of similarity across widths in earlier layers but large variation in deeper layers, which is the opposite trend to that observed for non-robust networks.

is effective at ensuring that perturbed representations do not differ too significantly from benign ones, unlike for non-robust networks.

C.2 Adversarially perturbed representations of non-robust networks

When analyzing the architectural impacts on learned representations using benign data, Nguyen et al. [42] note the emergence of a block structure with increased width and depth. We find that a much stronger block structure emerges even for low-width networks when using adversarial inputs (Fig. 23). This implies that perturbations force representations within a residual block to have higher similarity than outside the block. The block structure has been linked to the capacity of models, with Nguyen et al. [42] noting that the 'block structure arises in models that are heavily overparametrized relative to the training dataset'. In this light, adversarial examples have a peculiar

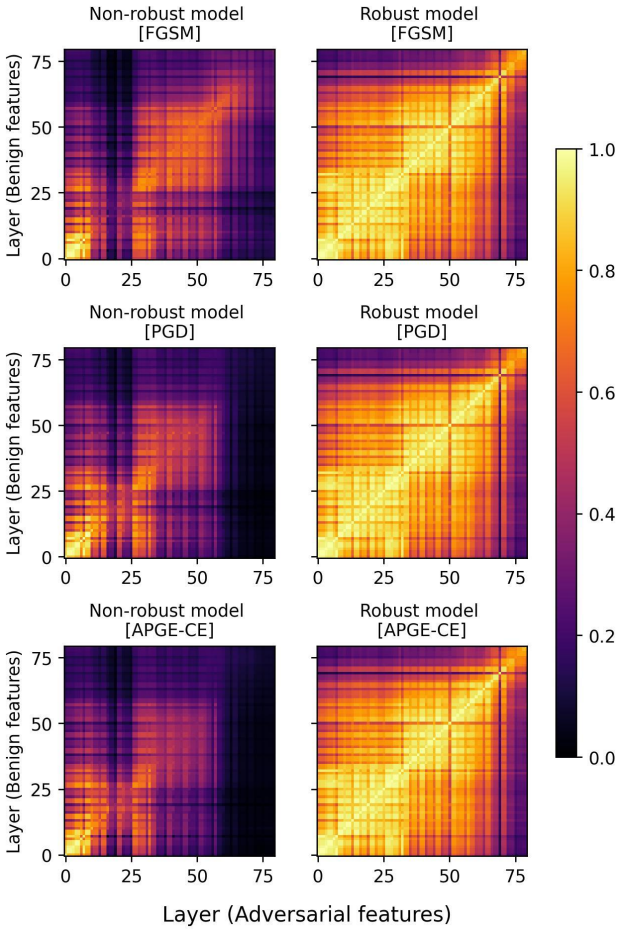

Figure 17: **Choice of adversarial attack**. We consider three different attacks, namely FGSM, PGD, and APGD-CE (arranged in order of attack strength) in this experiment. With each attack, we measure the cross-layer similarity between adversarial and benign representations. Our results show that such cross-layer similarity shows a similar trend across attacks, showing that our observation is agnostic to attack design choice.

impact on the representations of benign models, since the block structure is more clearly visible for adversarial inputs, but for models which do not classify the inputs correctly. This indicates that local similarity is being exhibited and is a different phenomenon compared to block structure emergence for well-trained models.

Figure 24 shows the stark difference between perturbed features for robust and non-robust networks. This is similar to the lack of similarity for benign inputs to these networks.

D Evolution over Training

In this section, we study the similarity between the activations produced by models after each epoch of training. We present our results in two formats, time series and heatmaps. For ease of understanding, the time series corresponds to a single row of the heatmap, where the representation being compared to is held constant.

D.1 Impact of Model Capacity

In Figure 25, we plot the pairwise similarity between the representations of a single layer after each epoch of training. Natural training behaves as we would expect it to: a layer's representations at a

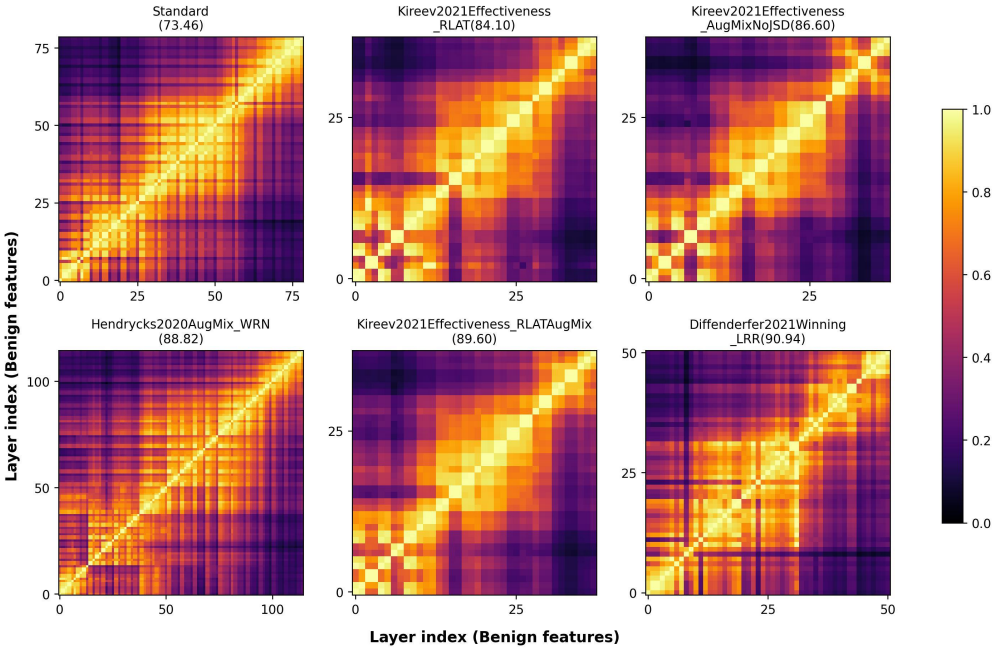

Figure 18: **Robustness to image corruptions**. While the main focus of this work is to investigate robust representation for worst-case adversarial attacks, we also investigate representations learned by networks robust to only common corruptions (such as photometric and weather changes). We consider multiple networks from the RobustBench [7] leaderboard that achieve better performance than a non-robust network on the CIFAR-C [23] dataset. We find that the difference between representations of the robust and non-robust networks is not as pronounced in the case of common corruption robustness. It suggests that the divergence of representations in non-robust and robust networks further depends on the strength of attack threat model.

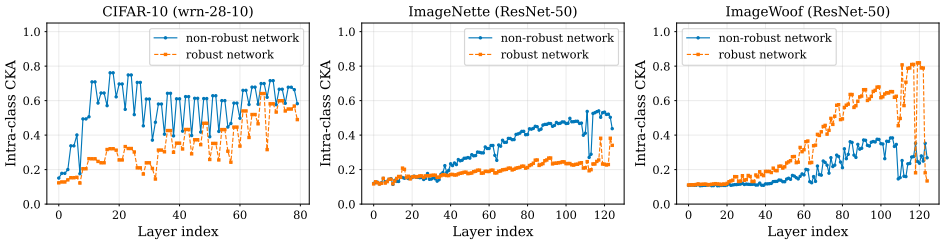

Figure 19: **Intra-class similarity.** We find that the contribution of intra-class similarity, measured by intra-class CKA, increases to non-trivial fraction, as we go deeper into the network.

given epoch are most similar to those from nearby epochs, and similarity degrades as the distance between epochs increases. Higher average similarity between later epochs implies convergence to a final learned representation. This pattern is also observed in the robust training of low-capacity networks, but as capacity increases starkly different dynamics emerge. In high-capacity robust networks, we observe similarity start to decrease after about 30 epochs of training, only to increase again later on. This pattern is observed for both benign and adversarial activations.

D.2 Adversarial Training and Overfitting

In Figure 26, we plot the similarity to the final learned representations of the representations extracted from each of the three Wide ResNet blocks (block1, block2, block3) and the final average pooling layer before classification (avgpool) after each epoch of training. We also plot the validation loss of each model for comparison. We find that for models trained at $\epsilon = \frac{8}{255}$, instability in the later layers is not observed until the model begins to overfit on adversarial examples. At high perturbation

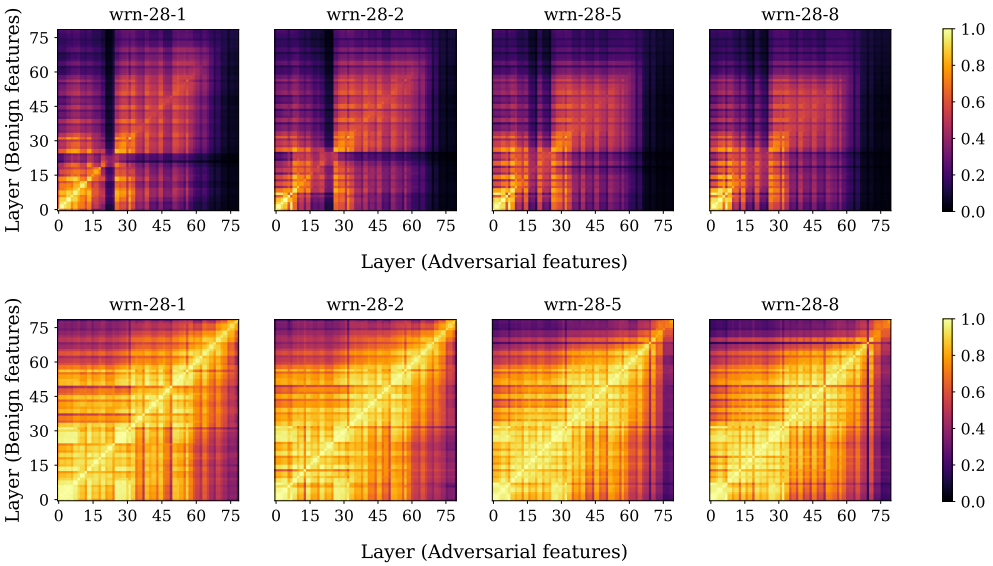

Figure 20: **Adversarial examples cause representation drift in later layers.** In the similarity plots of non-robust network representations (*top row*), adversarial and benign features display a similar structure to plots comparing just benign representations of non-robust models only in the early layers. In later layers, adversarial representations are very dissimilar from the benign representation of all layers. The similarity plots of robust networks (*bottom row*) are quite similar to plots comparing just benign representations of robust models, suggesting that robust networks learn similar representations for benign and adversarial data.

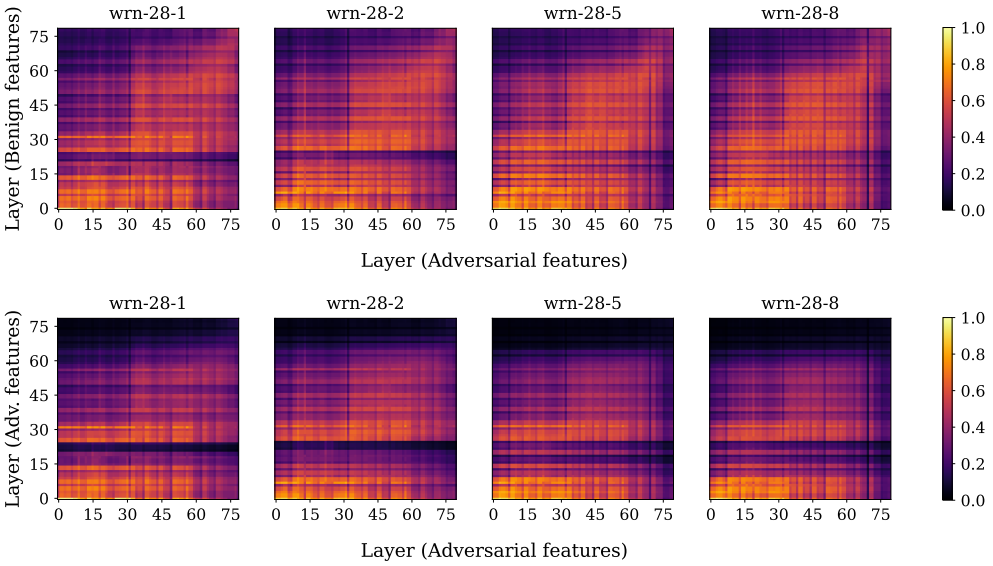

Figure 21: **Non-robust and robust models differ substantially across layers for both benign and perturbed inputs.** Cross layer CKA between a non-robust model (Y-axis) and robust model (X-axis) using perturbed and non-perturbed features.

strengths, training instability is observed at earlier layers and earlier in training. Training of the lowest capacity model is stable at all perturbation strengths, a trend also observed in Figure 25.

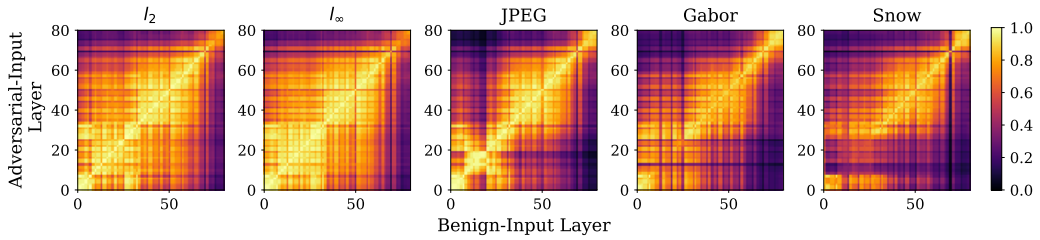

Figure 22: **Robustly trained models across threat models have aligned benign and perturbed representations.** Except the 'Snow' threat model, all the others have identical benign and perturbed representations across layers.

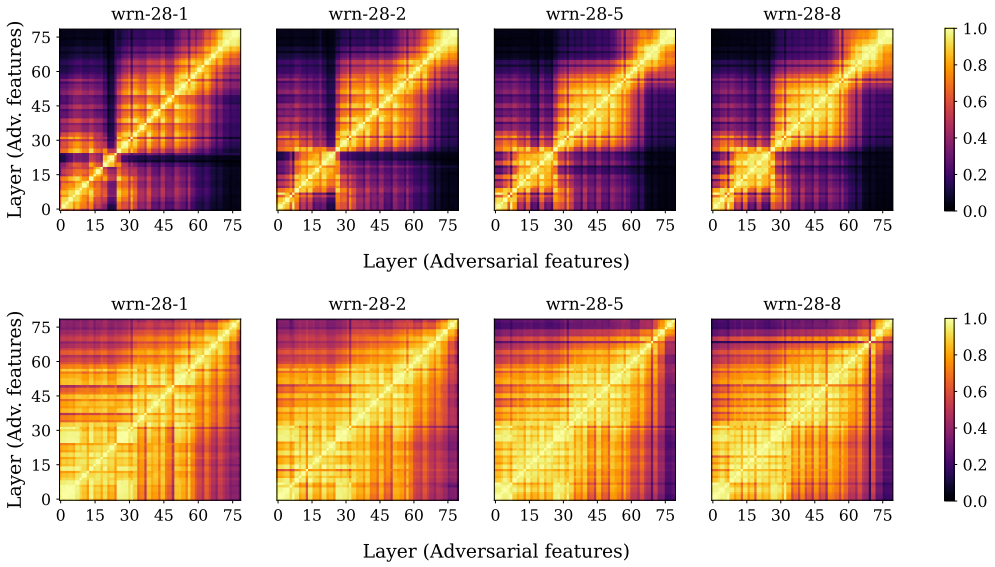

Figure 23: **Adversarial examples have different impacts on the representations of benign and robust models.** In benign models (top row), the layerwise similarity between adversarial activations displays a similar structure to that of benign activations, except the layers with dissimilar benign activations appear to have even more dissimilar robust activations. This implies significant changes in adversarial activations are taking place in between the self similar layer "blocks". This pattern is largely absent from robust models (bottom row), which display similar patterns for both benign and adversarial inputs.

D.3 Different Training Methods

We also sought to test whether more principled robust training methods, such as those proposed by Zhang et al. [65], would affect the patterns in similarity we observed in this section. In Figure 6, we compare benign training, PGD training, and TRADES training in a similar manner to Figure 26. The patterns we observed with PGD training disappeared when training with TRADES, highlighting the sensitivity of CKA to meaningful changes in training dynamics.

D.4 Training Dynamics of Different Threat Models

We extend our analyses from Section 5 to look at the Gabor and JPEG threat models. Results are plotted in Figure 27. We find that there are noticeable differences, especially in regards to overfitting observed in in ℓ_∞ training. However, across all threat models, we see that early layers are less affected by adversarial training.

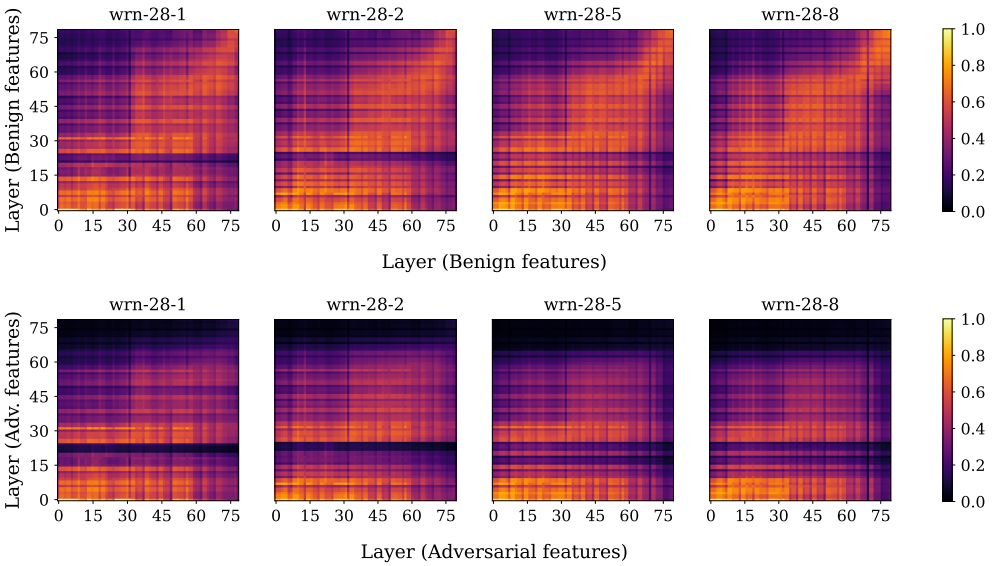

Figure 24: **Perturbed representations for robust and non-robust networks differ across all layers.** Cross layer CKA between a non-robust model (y-axis) and robust model (x-axis) using perturbed features.

D.5 Layer Freezing

Based off of the results of our experiments looking into the CKA analysis of training dynamics, we test whether those findings can be used to increase the efficiency of training. To test this, we froze the first block of a WRN-28-5 at different points in the first 40 epochs of training and recorded the maximum adversarial validation accuracy achieved over 100 epochs of training. As shown in Figure 29, when increasing the epoch freezing occurs at, accuracy starts off low (below 43%) and steadily increases until epoch 20, after which it levels off around 46-47%. This matches the trend of the CKA similarity convergence of convolutional layers within block 1 of a WRN-28-5 network, as shown in Figure 28. These results suggest that with knowledge of a network's training dynamics derived from CKA analysis, we can take a principled approach to layer freezing while maintaining a relatively high degree of accuracy.

E Threat models

In this section, we further investigate the impact of threat model on learned representations (see §7 in the main body).

E.1 Impact of budget within a threat model

In Figure 30, we show that even within a single attack, changing the budget leads to drastic changes in the representations at deeper layers.

E.2 Cross-threat model similarity

In Figure 31, we present a pairwise comparison of benign representations extracted from robust models trained on each of our threat models. This expands upon Figure 7 from the main body and demonstrates that while visual similarity leads to similar robust representations, the converse is not necessarily true. Snow and Gabor have similar representations in spite of being extremely visually different threat models (Fig. 8), demonstrating the value of using RS metrics to evaluate the viability of joint robust training.

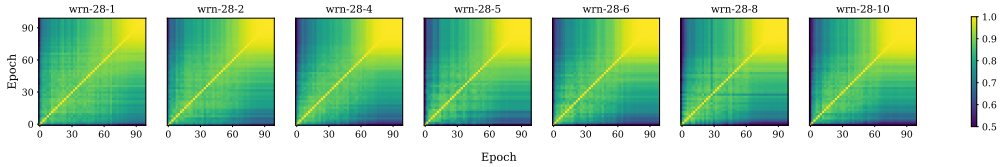

(a) *Non-robust* networks. Features extracted over *benign* images.

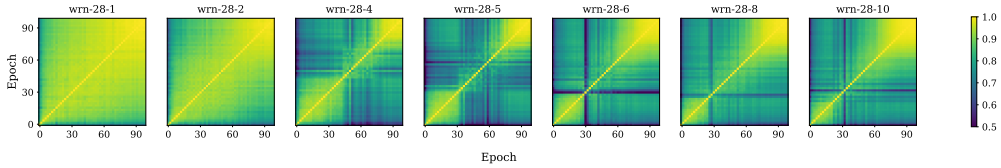

(b) *Robust* networks. Features extracted over *benign* images.

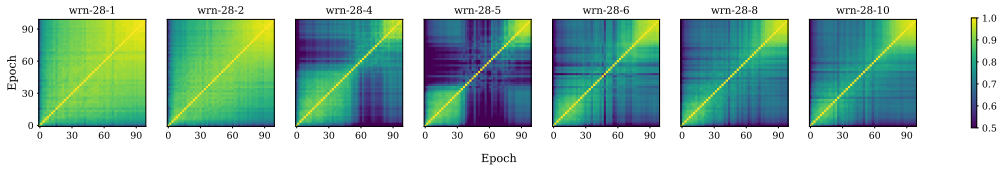

(c) *Robust* networks. Features extracted over *adversarial* images.

Figure 25: **Stability of robust training is impacted greatly by model capacity.** Each plot shows the CKA similarity between the activations of the final layer of a Wide ResNet feature extractor at each epoch of its 100-epoch training. While the stability of non-robust training is largely unaffected by capacity, the robust training of models above a certain capacity causes representations to be learned in the middle of training that are starkly different from the initial and final representations. This effect is even more pronounced when comparing adversarial representations.

E.3 Aligning representations across threat models

Figures 32 to 36 ablate on the results of Figure 31 by varying the perturbation size of each threat model used during training. As expected, models at lower budgets tend to be better aligned. At larger budgets, even for visually similar attacks like JPEG and ℓ_2, the aligment dips, particularly at deeper layers. This indicates that to train models jointly robust to different threat models, explicit constraints on learned representations during training may be needed.

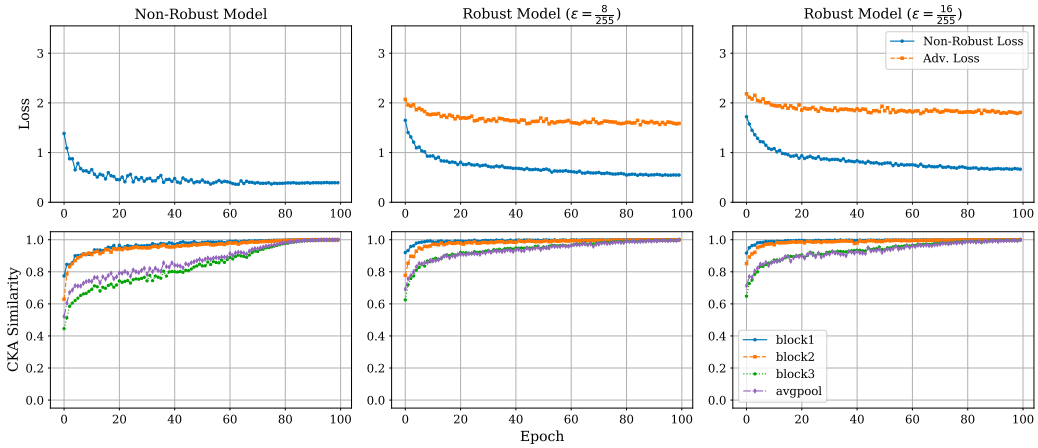

(a) WRN-28-1

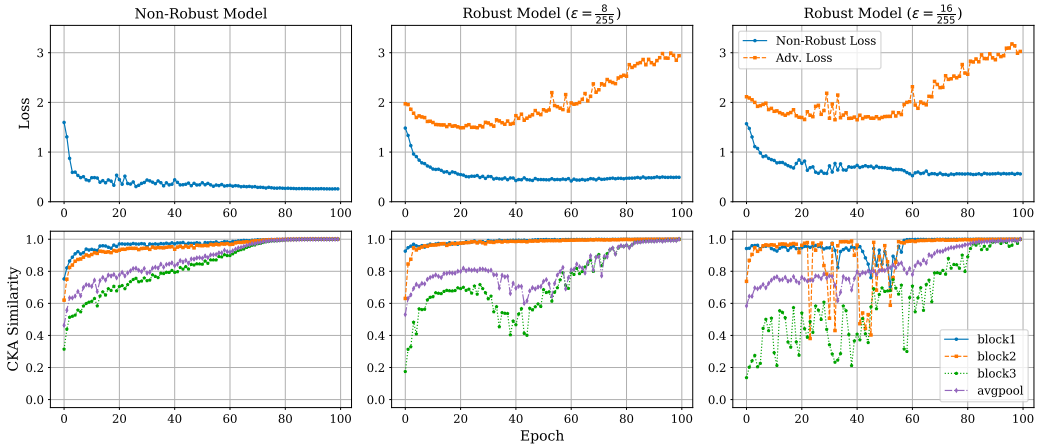

(b) WRN-28-5

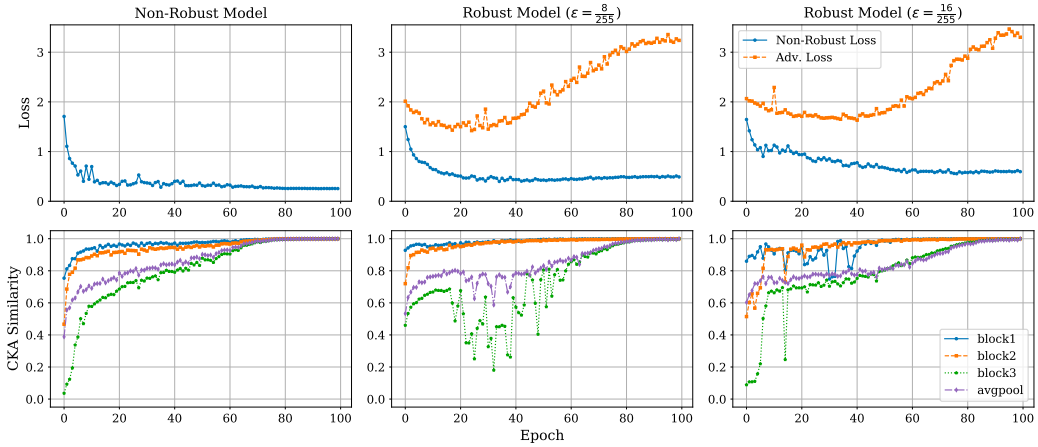

(c) WRN-28-10

Figure 26: **Overfitting and training instability in robust learning.** Each plot shows how benign representations of selected layers of Wide ResNet models compare to their final learned representations after each epoch of training. In larger robust models trained at $\epsilon = \frac{8}{255}$, training instability begins after the point of overfitting on adversarial data. However, when the perturbation strength is increased, there are large changes in the similarities of representations of subsequent epochs starting very early in training. High perturbation strengths also induce instability at earlier layers, which is not observed at lower strengths or in non-robust training.

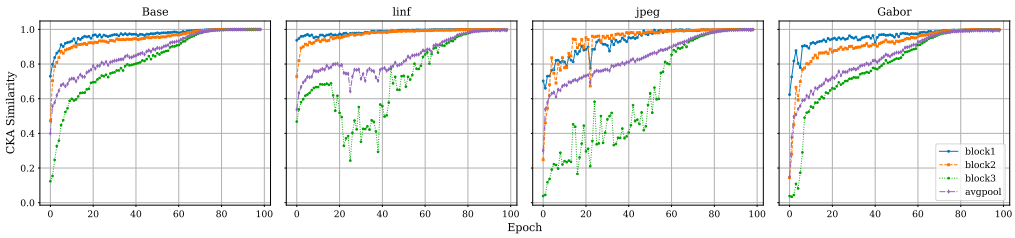

Figure 27: **Convergence of benign representations over robust training for different threat models.** Using CKA, we can observe differences in training dynamics between robust training for ℓ_∞, JPEG, and Gabor attacks. During JPEG-robust training, the output of block 3 appears to be even more significantly affected than in ℓ_∞ training, although the subsequent average pooling layer converges more smoothly. During Gabor training, the effects are more muted, possibly due to Gabor being a weaker attack.

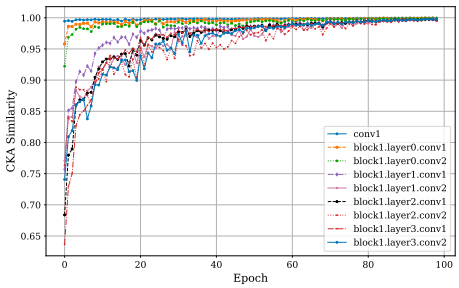

Figure 28: **Convergence of learned adversarial representations within block 1 of a robust WRN-28-5.** Zooming in on the first residual block, a clear elbow curve is present in the representations of all but the very first convolutional layers.

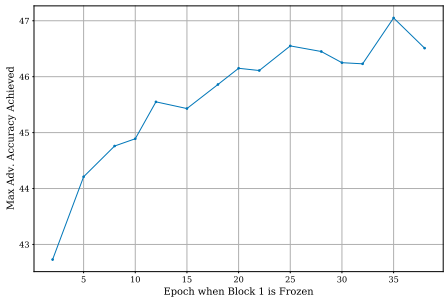

Figure 29: **Maximum adversarial validation accuracy after freezing early layers at various points during training.** Accuracies start low (43%) when the first block is frozen after 2 epochs of training, and steadily rise until around epoch 20, when robust accury levels off between 46 and 47%. This is similar to the pattern observed in Figure 28, in which the CKA similarity between the representations learned within block 1 at each epoch and the final representations level off around epoch 20.

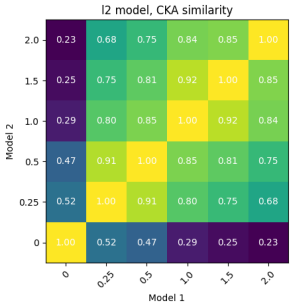

(a) ℓ_2

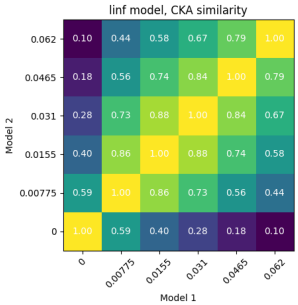

(b) ℓ_∞

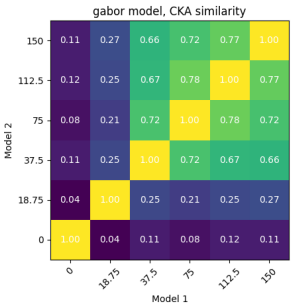

(c) Gabor

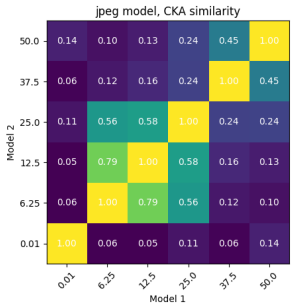

(d) JPEG

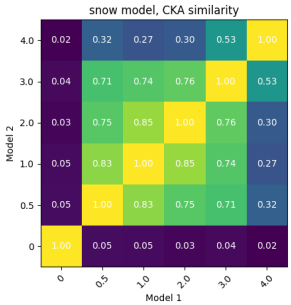

(e) Snow

Figure 30: **Adversarial training induces very different representations, even at low attack strengths.** Each plot displays the CKA similarity between activations of the final layer of WRN-28-10 feature extractors adversarially trained on different strengths of each threat model. In each plot, even the representations of the lowest strength robust model are quite dissimilar from those of the benign model, with only the ℓ_p bounded models having that similarity be relatively close to the lowest similarities between robust models.

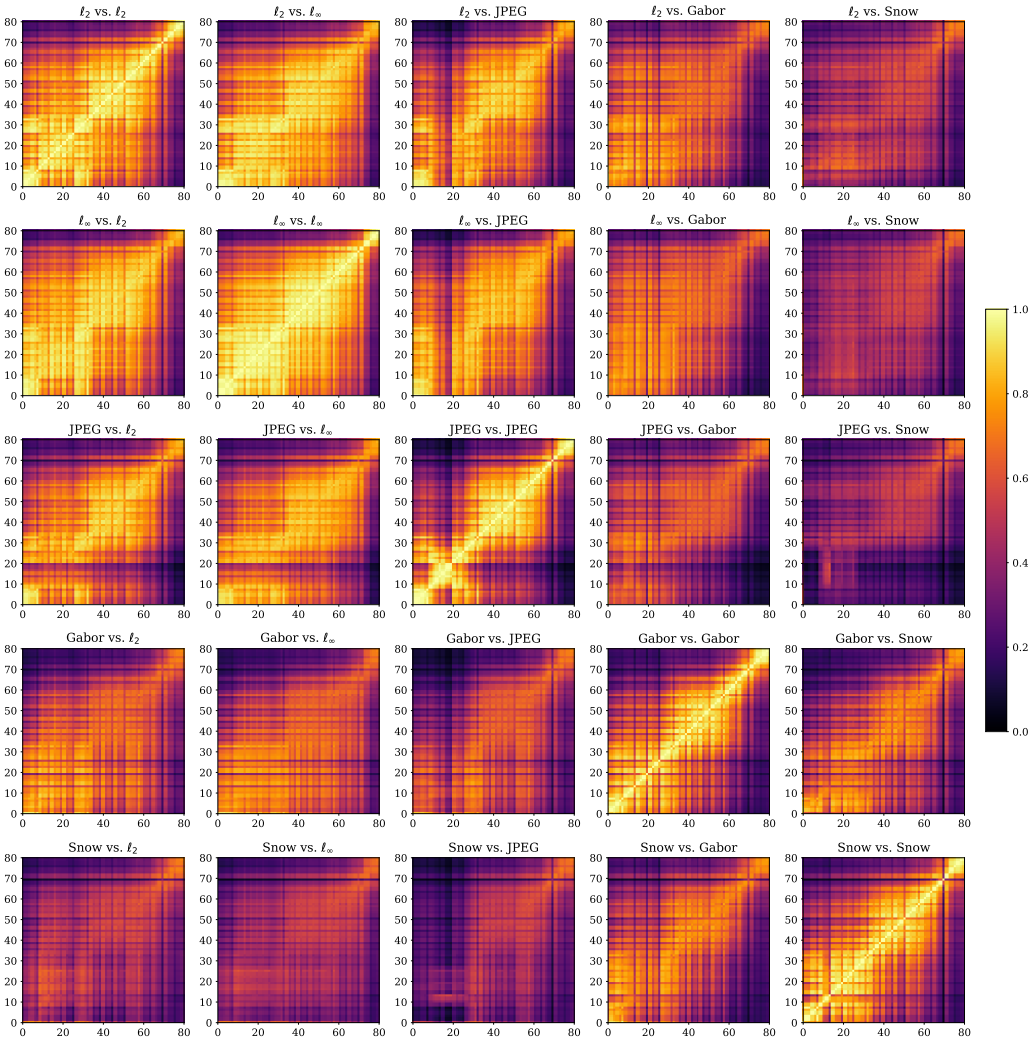

Figure 31: **Exploring relationships between threat models.** Each plot displays the layerwise similarity between benign activations of robust WRN-28-10 models trained against different threat models. As suggested by prior research [8], ℓ_p robust networks are shown to be highly similar. JPEG, which is ℓ_p bounded in the compression space, is also noticeably more similar to the ℓ_p bounded attacks than to the others. Interestingly, Snow and Gabor trained models are noticeably more similar to each other than to the other models, implying an unknown similarity between the classes of attack.

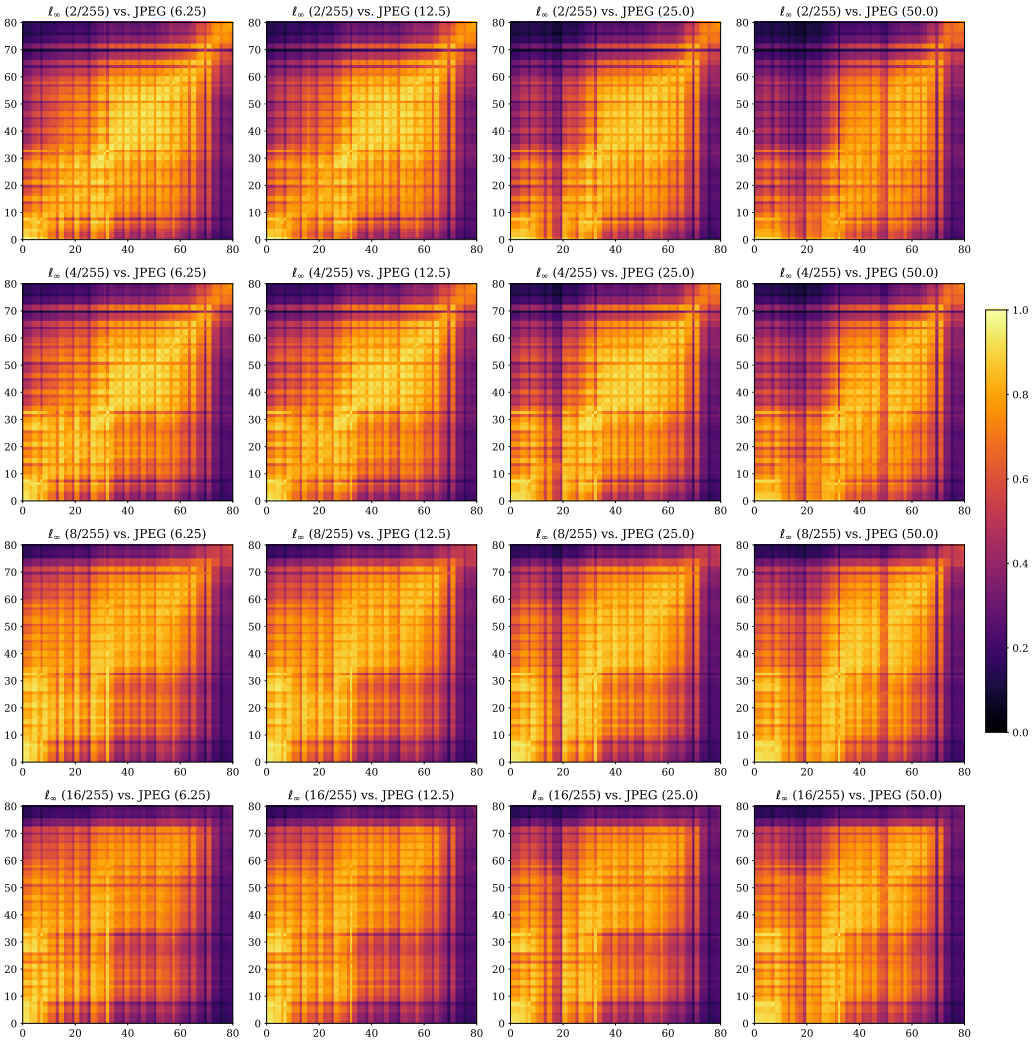

Figure 32: Comparing representations of l_∞ and jpeg robust models at different attack strengths.

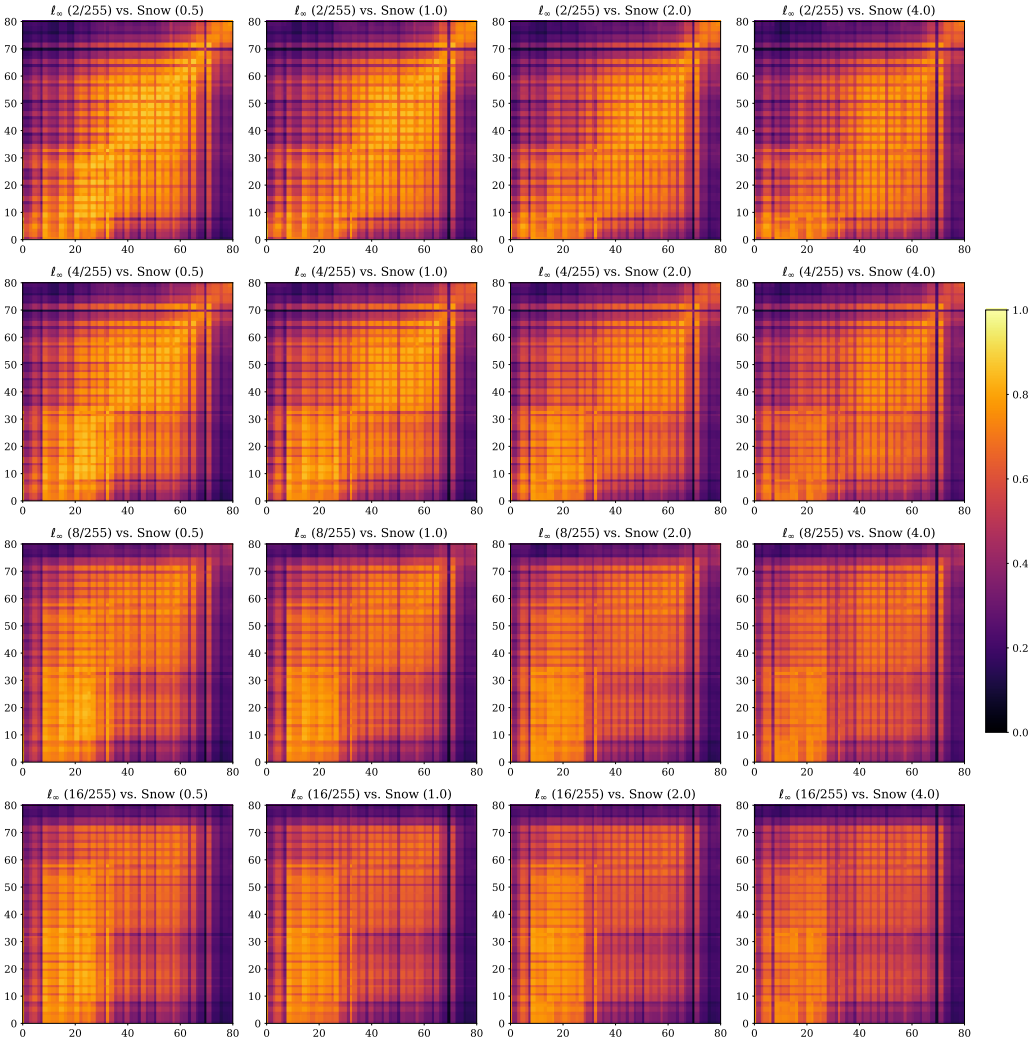

Figure 33: Comparing representations of l_∞ and snow robust models at different attack strengths.

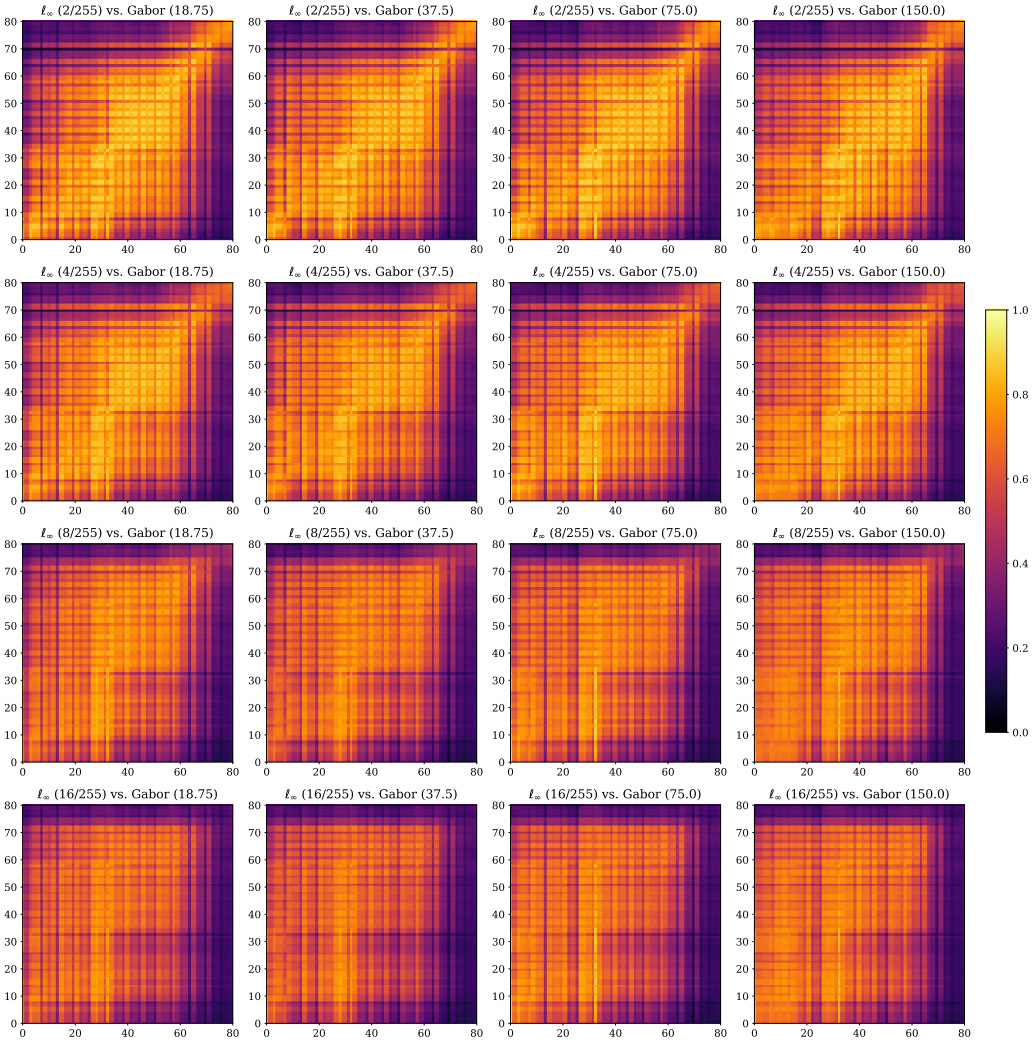

Figure 34: Comparing representations of l_∞ and gabor robust models at different attack strengths.

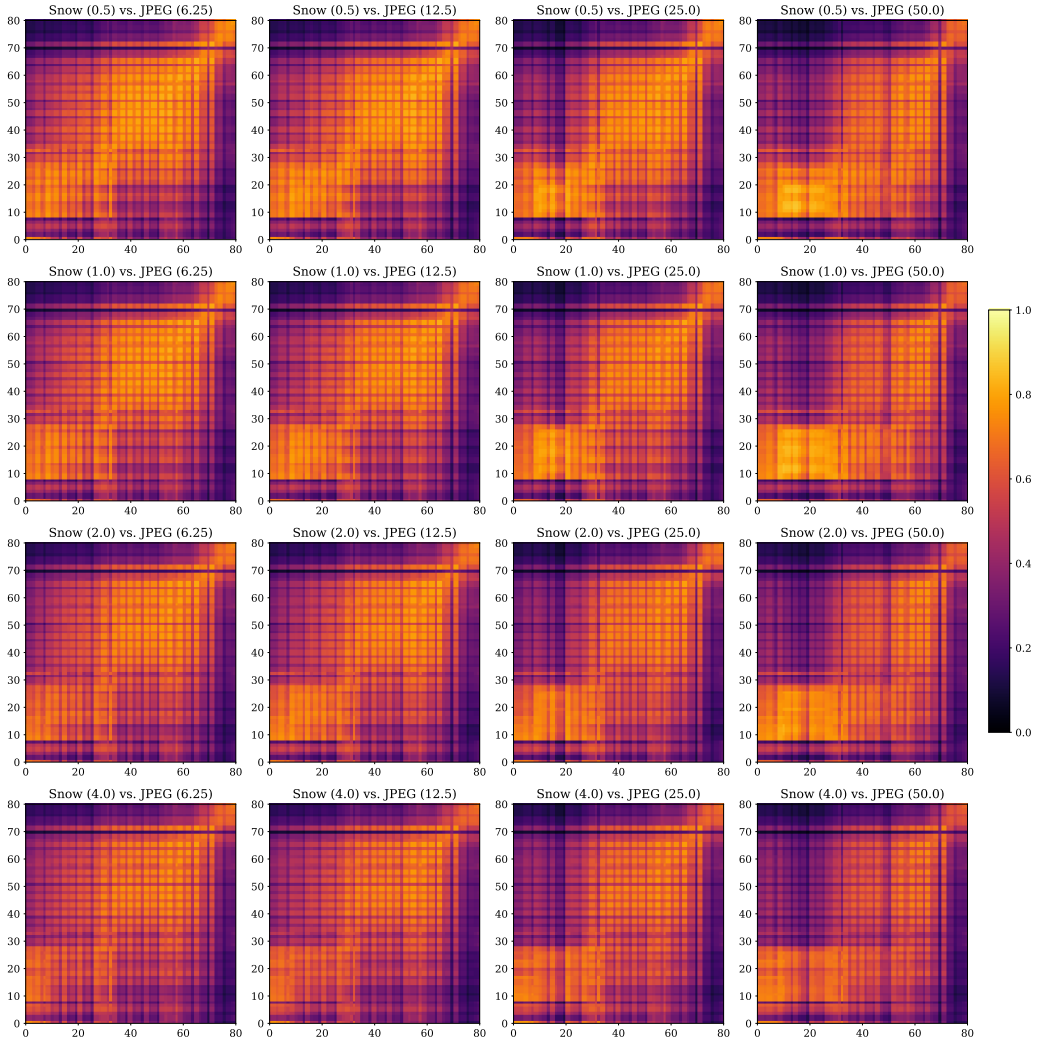

Figure 35: Comparing representations of snow and jpeg robust models at different attack strengths.

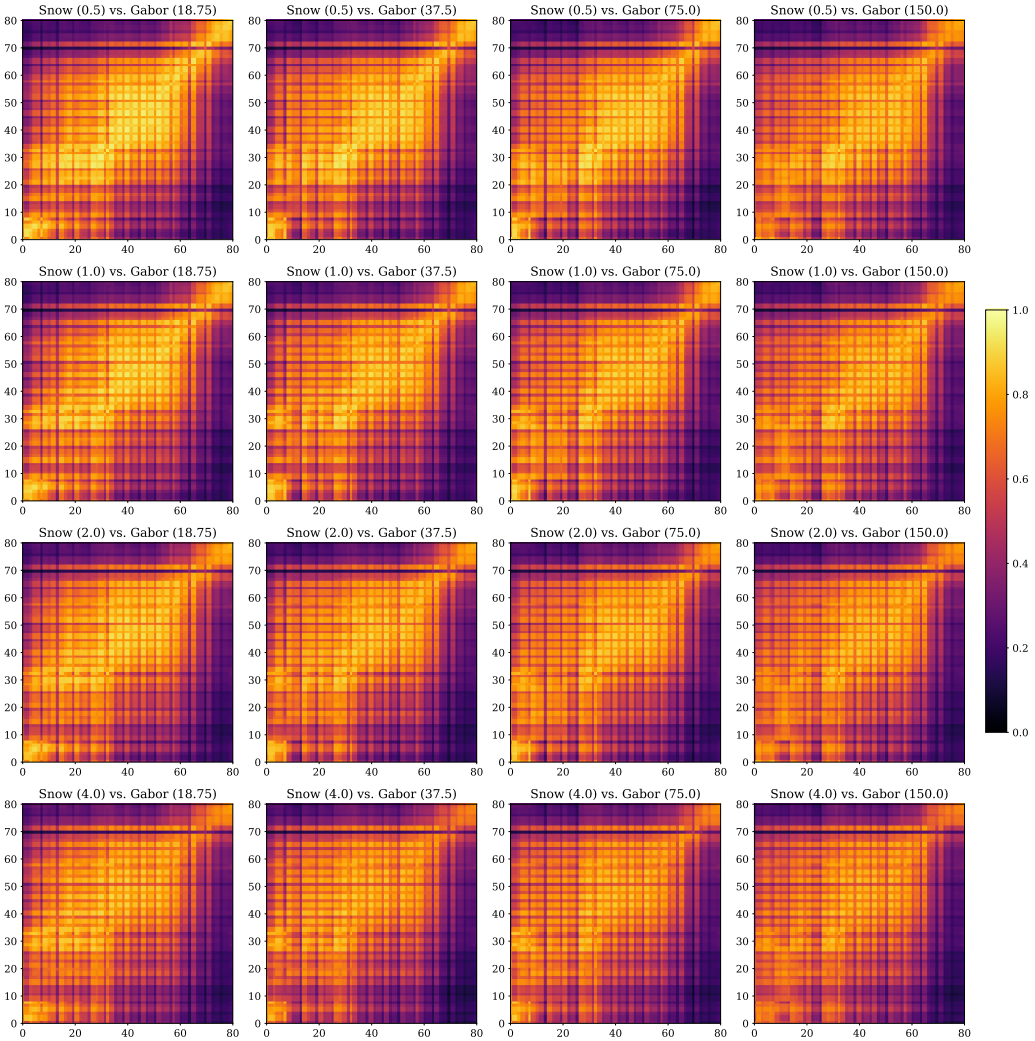

Figure 36: Comparing representations of snow and gabor robust models at different attack strengths.